HHS Public Access

Author manuscript

Cell Rep. Author manuscript; available in PMC 2020 March 06.

Published in final edited form as:

Cell Rep. 2020 January 21; 30(3): 932–946.e7. doi:10.1016/j.celrep.2019.12.062.

Transcriptional Programming of Human Mechanosensory Neuron Subtypes from Pluripotent Stem Cells

Alec R. Nickolls[1,2], **Michelle M. Lee**[1], **David F. Espinoza**[1], **Marcin Szczot**[3], **Ruby M. Lam**[2,3], **Qi Wang**[4], **Jeanette Beers**[4], **Jizhong Zou**[4], **Minh Q. Nguyen**[5], **Hans J. Solinski**[5], **Aisha A. AlJanahi**[4], **Kory R. Johnson**[1], **Michael E. Ward**[1,6], **Alexander T. Chesler**[3,6,*], **Carsten G. Bönnemann**[1,6,7,*]

[1]National Institute of Neurological Disorders and Stroke, National Institutes of Health, Bethesda, MD 20892, USA

[2]Department of Neuroscience, Brown University, Providence, RI 02912, USA

[3]National Center for Complementary and Integrative Health, National Institutes of Health, Bethesda, MD 20892, USA

[4]National Heart, Lung, and Blood Institute, National Institutes of Health, Bethesda, MD 20892, USA

[5]National Institute of Dental and Craniofacial Research, National Institutes of Health, Bethesda, MD 20892, USA

[6]Senior author

[7]Lead Contact

SUMMARY

Efficient and homogeneous *in vitro* generation of peripheral sensory neurons may provide a framework for novel drug screening platforms and disease models of touch and pain. We discover that, by ovesssrexpressing *NGN2* and *BRN3A*, human pluripotent stem cells can be transcriptionally programmed to differentiate into a surprisingly uniform culture of cold- and mechano-sensing neurons. Although such a neuronal subtype is not found in mice, we identify molecular evidence for its existence in human sensory ganglia. Combining *NGN2* and *BRN3A* programming with neural crest patterning, we produce two additional populations of sensory neurons, including a specialized touch receptor neuron subtype. Finally, we apply this system to

*Correspondence: alexander.chesler@nih.gov (A.T.C.), carsten.bonnemann@nih.gov (C.G.B.).

AUTHOR CONTRIBUTIONS

A.R.N., M.E.W., A.T.C., and C.G.B. conceived and designed the study. A.R.N., M.M.L., and D.F.E. developed the engineered iPSC lines and performed cell culture, PCR, and microscopy experiments. A.R.N., M.S., and R.M.L. performed electrophysiology and calcium imaging. M.Q.N. contributed to the single-nuclei RNA sequencing and analysis. J.Z. and Q.W. generated the PIEZO2 knockout iPSC line. J.B. reprogrammed the PIEZO2^{LOF} patient iPSC lines. H.J.S. contributed to the adult human DRG RNA *in situ* hybridization experiments. A.R.N., A.A.A., and K.R.J. performed the bulk RNA sequencing analysis. A.R.N. wrote the manuscript, and all authors edited the manuscript.

DECLARATION OF INTERESTS

The authors declare no competing interests.

SUPPLEMENTAL INFORMATION

Supplemental Information can be found online at https://doi.org/10.1016/j.celrep.2019.12.062.

model a rare inherited sensory disorder of touch and proprioception caused by inactivating mutations in *PIEZO2*. Together, these findings establish an approach to specify distinct sensory neuron subtypes *in vitro*, underscoring the utility of stem cell technology to capture human-specific features of physiology and disease.

In Brief

Nickolls et al. develop a method, using human stem cells, to generate specific types of sensory neurons that detect cold temperature and mechanical force. This approach uncovers a class of neuron found in humans, but not mice, and enables the modeling of a rare sensory disorder of touch and proprioception.

Graphical Abstract

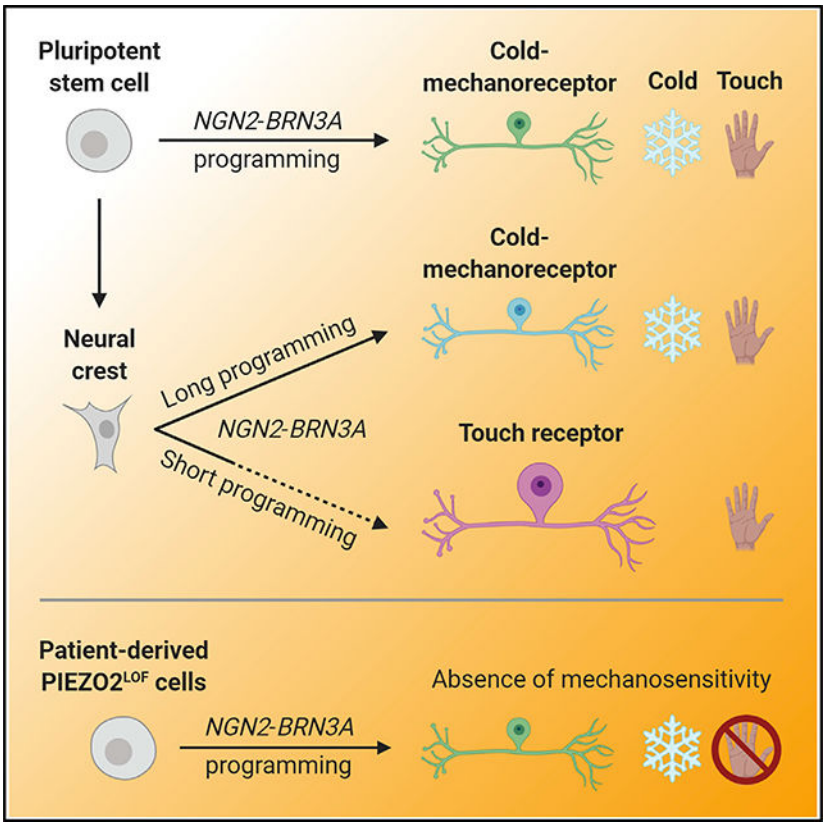

INTRODUCTION

The application of stem cell technology to the field of sensory biology promises unparalleled experimental access to the cells and molecules underlying human touch and pain. Further development in this area may enable novel drug screening approaches for chronic pain and facilitate more relevant modeling of disease. However, human peripheral sensory neurons are particularly challenging to recreate *in vitro* because they are an inherently heterogenous cell population. *In vivo*, their cell bodies reside in peripheral ganglia, which contain a rich array of functionally disparate neuron subtypes. Sensory neurons establish synapses in the

spinal cord and send long processes to peripheral targets, such as the skin (Moehring et al., 2018). There, they form specialized nerve endings that transduce environmental stimuli into electrical signals that are relayed back to the spinal cord and brain.

Peripheral sensory neurons can be functionally grouped into at least three broad categories (Lallemend and Ernfors, 2012): (1) low-threshold mechanoreceptors (LTMRs) are responsible for the mechanotransduction of innocuous forces, including vibration, discriminative touch, and gentle brushing; (2) proprioceptors are a distinct class of mechanosensory neuron specialized to convey information about joint angle and body position; and (3) nociceptors and thermoreceptors are tuned to sense painful or thermal stimuli, including damaging mechanical force, noxious chemicals, heat, and cold. Nociceptor and thermoreceptor neurons can be further broken down into discrete subtypes with overlapping and often polymodal functional properties.

Although the basic signaling pathways in sensory neuron development are known, the transcriptional and environmental factors underpinning the extraordinary subtype diversity of these neurons remain mysterious (Lallemend and Ernfors, 2012). Furthermore, whether it is possible to derive a pure population of an individual sensory subtype *in vitro* is a major unresolved question. Methods exist to produce human sensory neurons from pluripotent stem cells (Alshawaf et al., 2018; Chambers et al., 2012; Jones et al., 2018; Schrenk-Siemens et al., 2015; Schwartzentruber et al., 2018). However, these protocols require complex and varied media formulations to accurately direct stem cell differentiation by chemical means, and they can yield heterogeneous or ill-defined sensory neuron populations.

Recently, forced expression of specific neural transcription factors has been shown to directly reprogram mouse and human fibroblasts to resemble peripheral sensory neurons (Blanchard et al., 2015; Wainger et al., 2015). The resulting induced sensory neurons (iSNs) are functional but also heterogeneous, and they represent a minority of the total cells in culture. However, similar approaches that instead use induced pluripotent stem cells (iPSCs) as a starting population have shown remarkably high induction rates of cortical or motor neuron types depending on the transcription factors used (Mazzoni et al., 2013; Yang et al., 2017; Zhang et al., 2013). Neuronal differentiation performance can be further maximized by engineering iPSC lines with genomically integrated constructs harboring doxycycline-inducible transcription factors (Mazzoni et al., 2013; Wang et al., 2017; Fernandopulle et al., 2018).

Here, we applied a genome engineering strategy to establish a human iPSC-based sensory neuron differentiation method, utilizing the transcription factors *NGN2* and *BRN3A*. Stably integrating an inducible construct into the genome of iPSCs allowed for the controlled co-expression of *NGN2* and *BRN3A*. A previous study has demonstrated that these two transcription factors, when simultaneously delivered via separate lentiviral vectors, can reprogram a fraction of fibroblasts into a mixed culture of sensory neuron subtypes (Blanchard et al., 2015). By contrast, we found that our approach selectively converts iPSCs into a homogeneous culture of a single sensory neuron subtype, able to transduce both cold and mechanical stimuli. Although this neuronal subtype has not been observed in mice

(Nguyen et al., 2017; Szczot et al., 2017), we validated the existence of similar neurons in adult human tissue. By combining the forced expression of *NGN2* and *BRN3A* with a traditional neural crest differentiation protocol, we were able to produce two additional sensory neuron subtypes, including a pure population of LTMRs. Lastly, we applied these methods to investigate the molecular basis of a rare neurogenetic human disorder, caused by loss-of-function mutations in the mechanosensitive ion channel *PIEZO2*. Patients with this condition present clinically with a profoundly impaired sensation of vibration, gentle touch, and proprioception. These data establish transcriptional programming of iPSCs as a means to derive functionally homogeneous sensory neurons *in vitro*, which reflect human-specific cell types and enable human disease modeling.

RESULTS

NGN2-BRN3A Programming in iPSCs Induces a Peripheral Sensory Neuron Phenotype

Fibroblasts can be converted into peripheral sensory neurons at approximately 5%–10% efficiency by forced overexpression of the transcription factors *NGN2* and *BRN3A* (Blanchard et al., 2015). With the goal of designing a simple yet effective sensory neuron induction system, we created an expression cassette containing the coding sequences of *NGN2* and *BRN3A* (*NGN2-BRN3A*) separated by a T2A ribosomal-skipping peptide and under the control of a doxycycline-inducible promoter (Figure S1A). This strategy enables equimolar and regulated expression of both factors in tandem (Das et al., 2016; Liu et al., 2017). The vector also contained homology arms against the *CLYBL* genomic safe-harbor site. We chose *CLYBL* because of its greater capacity for stable transgene expression, as compared with other loci such as *AAVS1* (Cerbini et al., 2015). Using a characterized pair of transcription activator-like effector nucleases (TALENs) targeting the *CLYBL* locus (Cerbini et al., 2015), we genetically engineered a control human iPSC line (WTC11) (Miyaoka et al., 2014) to stably harbor the *NGN2-BRN3A* construct by homology-directed repair. The construct included a constitutively expressed EGFP reporter and puromycin resistance, flanked by loxP sites. These allowed for visual identification and drug selection of stably integrated, single-cell-derived iPSC colonies. This was followed by Cre recombinase treatment to excise the reporter and selection genes (Figure S1B). Targeted insertion of the *NGN2-BRN3A* construct was verified by PCR genotyping (Figure S1C). With the aim of achieving robust transgene expression, we used only clones with insertion at both *CLYBL* alleles for further experiments. To test the expression activity of the transgene, we supplemented doxycycline to the culture medium and assayed *NGN2-BRN3A* expression by RT-PCR (Figure S1D). At baseline, transgene expression was undetectable. However, the addition of doxycycline stimulated *NGN2-BRN3A* transcription within 48 h, which was reversible upon withdrawal of the drug.

NGN2-BRN3A-engineered iPSCs exhibited normal growth characteristics in the absence of doxycycline, having roughly a 24-h doubling time (Video S1). We next assessed cellular morphology over time with continuous presence of doxycycline in a neural growth medium. To avoid biasing lineage decisions, the medium was devoid of small-molecule inhibitors traditionally used for neural differentiation (see STAR Methods). Approximately 48 h after doxycycline application, we noticed a rapid loss of pluripotent morphology as the cells

physically separated from one another and synchronously ceased dividing (Figure 1A; Video S2). Over the next 5 days, the cells extended an elaborate network of processes. By day 14, the culture reached a stable, uniform neuronal appearance with large, rounded soma morphologies. We observed reduced differentiation efficiency and increased cell death when doxycycline was withdrawn before this time point (data not shown), so all described experiments include doxycycline for the first 14 days of differentiation.

We compared these cultures with neurons induced with *NGN2* expression alone, which produces a glutamatergic cortical layer 2/3 neuron population (Figure 1A; Zhang et al., 2013; Wang et al., 2017). Compared with *NGN2-BRN3A*-induced neurons, *NGN2*-induced neurons showed subtle differences in differentiation speed and morphology, extending bipolar processes by day 4 and ultimately adopting a more angular soma consistent with a pyramidal neuron identity. Both *NGN2-BRN3A* and *NGN2* neurons maintained their morphology upon withdrawal of doxycycline on day 14. By day 21, *NGN2-BRN3A*-induced cultures tended to form dense bundles of processes reminiscent of fasciculated axon tracts, which was not observed in *NGN2*-induced cultures (Figure 1B). Immunocytochemical analysis of both culture types revealed distinct expression patterns of the dendritic marker MAP2 and the intermediate neurofilament peripherin (PRPH), a protein abundantly found in the peripheral nervous system (Fornaro et al., 2008). Peripherin was selectively expressed in *NGN2-BRN3A* cultures, whereas MAP2 showed greater distribution in *NGN2* cultures, consistent with the elaborate dendritic arbor of central nervous system neurons (Figure 1B). Because *NGN2-BRN3A* neurons exhibited a mature neuronal morphology at this time point, further experiments were performed no earlier than 21 days after doxycycline induction (and 7 days after its withdrawal).

Peripheral axons can be defined by their diameter, in order from large to small: Aα, Aβ, Aδ, and C, with C fibers being unmyelinated. In mice, Nefh (NF200) is a heavy neurofilament specific to the myelinated fiber types Aα, Aβ, and Aδ. However, a recent analysis of NEFH in human dorsal root ganglia (DRG) demonstrated nearly universal fiber expression (Rostock et al., 2018). By contrast, peripherin is most highly expressed in unmyelinated C fibers and some Aδ fibers in both mice and humans (Fornaro et al., 2008; Holford et al., 1994; Vang et al., 2012). Thus, similar to human sensory ganglia C or Aδ fibers, we found extensive co-localization of NEFH and peripherin in *NGN2-BRN3A* neurons (Figure 1C). To further investigate the peripheral identity of *NGN2-BRN3A* neurons, we used antibodies against a neuronal nuclear marker (NeuN) and the transcription factors *BRN3A* and *ISL1* (Figure 1C), which are expressed in all sensory neurons *in vivo* (Dykes et al., 2011). Most of the culture population was labeled by these antibodies, indicating a near-complete conversion (Figure 1D).

Endogenous sensory neurons have a distinct repertoire of neurotrophin receptors based on their functional identity (Marmigère and Ernfors, 2007). In mice, nociceptor (pain) and thermoreceptor (temperature) neurons express the receptor TrkA, encoded by *Ntrk1* (Fang et al., 2005). Subtypes of LTMR (gentle touch) neurons express TrkB (*Ntrk2*) (Li et al., 2011), TrkC (*Ntrk3*) (Bai et al., 2015), or some combination (Nguyen et al., 2017). Proprioceptor (body position) neurons express only TrkC (Mu et al., 1993). Labeling *NGN2-BRN3A* neurons with antibodies against these receptor proteins revealed abundant and homogeneous

expression of TRKB, but minimal to no expression of TRKC and TRKA (Figure 1C), reminiscent of an Aδ LTMR subtype previously described in mice (Li et al., 2011).

The above experiments indicate that forced co-expression of *NGN2* and *BRN3A* for 14 days in human iPSCs efficiently generates cells that resemble a subset of peripheral sensory neurons. As with other neural lineage conversions, *NGN2-BRN3A* induction rapidly yields a neuronal morphology, likely bypassing some or all of the natural embryonic progenitor stages (Yang et al., 2017; Zhang et al., 2013). For this reason, we will refer to the converted cells as iSNs.

iSNs Express a Subset of Sensory Neuron Genes

To better define the iSN gene expression profile, and to determine to what degree they correspond to *in vivo* sensory neurons, we conducted RNA sequencing on bulk iSN cultures at day 21. Based on the expression of TRKB (*NTRK2*), we hypothesized that iSNs could represent a variety of LTMRs, which are a category of skin-innervating neurons responsible for transducing innocuous mechanical stimuli. In agreement with earlier immunocytochemistry results, *NTRK2*, but not *NTRK1* or *NTRK3*, was highly upregulated in iSNs relative to undifferentiated iPSCs (Figure 2A). In addition to the other markers assessed by antibody labeling, we observed a subset of neuronal genes enriched to a similar degree between iSNs and human donor DRG. Among genes involved in neurotransmitter synthesis, iSNs expressed the vesicular glutamate transporter *SLC17A7* (VGLUT1), suggesting an excitatory glutamatergic neuron identity. A variety of neurotransmitter receptor genes were also detected, including those for acetylcholine and GABA, and to a lesser extent, *N*-methyl-D-aspartate (NMDA), AMPA, and kainate-type glutamate receptor subunits.

Due to the current lack of detailed knowledge regarding human sensory neuron gene expression patterns, it is difficult to assign a specific endogenous subtype identity to an *in-vitro*-derived cell population. Relying primarily on information from the mouse literature, we examined gene transcripts that might infer the presence of different sensory neuron categories in iSN cultures. The voltage-gated sodium channel $Na_V1.7$, encoded by *SCN9A*, is ubiquitous in peripheral sensory neuron subtypes and is critical for the transmission of sensory stimuli in humans (Dib-Hajj et al., 2010). *SCN9A* was robustly expressed in iSNs, but not the nociceptor-specific *SCNA10A* ($Na_V1.8$) and *SCN11A* ($Na_V1.9$) (Figure 2A). Supporting a non-nociceptive identity, iSNs were devoid of most genes involved in pain, itch, and temperature sensation. Three notable exceptions were the inflammatory peptide substance P (*TAC1*), the purinergic receptor *P2RX3*, and the cold receptor *TRPM8* (Figure 2A).

Murine *Trpm8* is always co-expressed with TrkA and peripherin, representing a specific class of small- and medium-diameter fibers (Dhaka et al., 2008; Kobayashi et al., 2005; Takashima et al., 2007). In iSNs, the expression of *TRPM8* but the absence of TRKA precluded direct assignment to any known sensory neuron subtype (Figure 2A). We also found expression of *PIEZO2*, the mechanotransduction ion channel underlying proprioception and gentle touch sensation (Ranade et al., 2014; Woo et al., 2015). However, iSNs showed virtually no expression of *MAF* or *RUNX3*, which mark *PIEZO2*-expressing

Aβ LTMRs and proprioceptive neurons, respectively (Levanon et al., 2002; Wende et al., 2012). iSNs also had detectable levels of *NGN2* (*NEUROG2*), which is not found in the adult human DRG (Figure 2A). This could be an effect of residual doxycycline-induced *NGN2-BRN3A*. It can take up to 72 h for the transgenic RNA transcript to dissipate after doxycycline removal (Figure S1D), and transgenic *NGN2* is known to recruit expression of endogenous *NGN2* (Zhang et al., 2013). These unexpected gene expression patterns indicate that iSNs may represent an immature, artifactual, or otherwise unknown cell population that mimics certain features of native sensory neurons.

iSNs and Human DRG Neurons Co-express *TRPM8* and *PIEZO2*

Trpm8 and *Piezo2* are mutually exclusive in mouse sensory ganglia, highlighting a labeled line for cold sensation that is separate from mechanosensation (Knowlton et al., 2013; Nguyen et al., 2017; Szczot et al., 2017). Because our bulk iSN RNA sequencing dataset showed expression of both *TRPM8* and *PIEZO2*, we reasoned iSN cultures might be a mixture of neurons with non-overlapping expression of these two genes. We carried out RNA *in situ* hybridization on iSNs to determine the population distribution of *TRPM8* and *PIEZO2*, as well as lineage-defining neurotrophin receptor transcripts. Corroborating the previous immunocytochemistry and RNA sequencing experiments, *NTRK1* was absent, whereas *NTRK2* was prevalent, in essentially every cell (Figure 2B). *NTRK3* was also detectable across the entire population at a much lower level. Co-expression of the corresponding proteins TRKB and TRKC has been described in a subset of mouse DRG neurons (Fariñas et al., 1998). Surprisingly, the majority of iSNs also co-expressed *TRPM8* and *PIEZO2*, based on a conservative measurement of ≥ 5 labeled mRNA puncta of each transcript per cell (Figures 2B and 2C). With these criteria, we conclude that iSNs are a relatively homogeneous population that unexpectedly co-expresses *TRPM8* and *PIEZO2* in conjunction with *NTRK2* and low levels of *NTRK3*.

In the adult human DRG, *PIEZO2* is abundantly expressed (Rostock et al., 2018), but its relationship to *TRPM8* is unknown. We performed dual-label RNA *in situ* hybridization on DRG tissue from four unrelated human donors to assess the expression pattern of both genes (Table S1). DAPI was used, which most strongly labels non-neuronal satellite cell nuclei, in combination with the pan-neuronal gene *TUBB3* to identify individual neuron somas by *TUBB3*$^{+}$ circular recesses in the tissue (Figure S2A).

Among neurons labeled by *PIEZO2* and *TRPM8* probes, the majority expressed only *PIEZO2*, whereas a small fraction was exclusively marked by *TRPM8* (Figure 2D). Intriguingly, a large subset of neurons expressed both *PIEZO2* and *TRPM8*, as seen in the iSNs, and outnumbered those expressing only *TRPM8* (Figures 2D, 2E, and S2B). Furthermore, we found that some DRG neurons seem to express *TRPM8* with *NTRK2*, also like the iSNs, but the lower quality of our *NTRK2* labeling prevented rigorous quantification (Figure S2C). These findings suggest that the co-expression of TRPM8, PIEZO2, and NTRK2 might define a molecular class of sensory neuron found in humans, but not mice.

iSNs Detect Cold and Mechanical Stimuli

A sensory neuron that expresses *TRPM8* and *PIEZO2* should be equipped to transduce both cold and mechanical stimuli. We used the calcium dye Fluo-4 to monitor iSN calcium activity in real time at different temperatures. Shifting the recording medium from 25°C to 4°C induced a robust and sustained calcium influx across the entire culture (Figures 3A–3C). The *TRPM8* inhibitor RQ-00203078 reversibly blunted the calcium response. By contrast, application of 50°C heat had no effect on iSN activity (Figures 3B and 3C).

Menthol is a chemical chilling agent from mint plants that is a natural ligand of TRPM8 (McKemy et al., 2002; Peier et al., 2002). Application of this compound elicited a calcium response similar to cold temperature (Figures 3B and 3C; Video S3). We also evaluated other pungent chemicals targeting different TRP channels. Allyl isothiocyanate (AITC) from mustard plants is a ligand of TRPA1 (Bandell et al., 2004; Jordt et al., 2004), and capsaicin from chili peppers is a ligand of the heat-sensing channel TRPV1 (Caterina et al., 1997). Consistent with the absence of these ion channels in the RNA sequencing data, iSNs showed essentially no response to AITC and capsaicin (Figures 3B and 3C). Some neurons exhibited minor calcium transients in the presence of AITC, which can be attributed to its additional role as a weak TRPM8 agonist (Figure 3C; Janssens et al., 2016). Based on the expression of the purinergic receptor *P2RX3* in iSNs, we tested the P2RX3 ligand α,β-methylene-ATP, a molecule that induces chronic pain in mice (Cook et al., 1997; Inoue et al., 2003). Application of α,β-methylene-ATP did not produce a sustained calcium influx, but the basal rate of iSN spontaneous activity drastically increased (Figures 3B and 3C). This type of response is likely due to the fast inactivation of the P2RX3 channel (Cook et al., 1997).

Next, we used whole-cell patch clamp to assess iSN electrophysiological properties. In current clamp, resting potential was generally between −55 and −65 mV, and action potential trains were elicited by current injection (Figure 3D). Bath application of tetrodotoxin completely blocked action potential generation. This is consistent with absence of the tetrodotoxin-resistant sodium channels $Na_V1.8$ and $Na_V1.9$, which are exclusive to nociceptors (Dib-Hajj et al., 2010).

Resting potential was held at −60 mV in voltage clamp and the cell membrane was indented by a blunt probe to interrogate the mechanosensitivity of iSNs (Figure 3E; Video S4). We observed an inward current with rapid inactivation kinetics that increased in amplitude with greater indentation (Figures 3E and 3F). Mechanically activated, rapidly adapting currents are found in a variety of sensory neurons that mediate touch detection (Iggo and Ogawa, 1977). Genetic deletion of *PIEZO2* in mice and in human iPSC-derived LTMRs ablates these currents (Ranade et al., 2014; Schrenk-Siemens et al., 2015). Given that the iSNs here manifest a similar current and express *PIEZO2*, this ion channel is likely the molecular transducer underlying iSN mechanosensitivity.

Varied Induction of NGN2-BRN3A Expression in Neural Crest Yields Divergent Sensory Neuron Populations

The most common sensory neuron differentiation methods use small-molecule inhibitors in a stepwise protocol to guide iPSCs through the natural stages of embryonic development,

first reaching a neural crest progenitor stage before terminal differentiation (Alshawaf et al., 2018; Chambers et al., 2012; Jones et al., 2018; Schwartzentruber et al., 2018). However, the forced expression of lineage-specific transcription factors has recently been applied to directly induce fibroblasts into sensory neurons (Blanchard et al., 2015; Wainger et al., 2015). We wondered whether such transcriptional programming of iPSCs using a generic sensory neuron code, in the absence of natural developmental patterning signals, might be responsible for the unusual gene expression profile of our iSNs.

To test the above hypothesis, we adapted an established method to first differentiate iPSCs into neural crest cells (Bajpai et al., 2010), which are the multipotent stem cells that naturally give rise to peripheral sensory neurons *in vivo*. Only a small fraction of neural crest cells spontaneously differentiates toward a sensory neuron fate *in vitro* (data not shown) (Schrenk-Siemens et al., 2015). Therefore, we evaluated the combined effect of our iSN conversion protocol with neural crest development. Similar to iPSCs, exposure of neural crest to doxycycline for 14 days caused a rapid and uniform differentiation to a neuronal morphology (Figure 4A). We will refer to these cells as neural crest-derived iSN population 1 (NC-iSN1).

During sensory development in mice, the neurogenic factor NGN2 is transiently upregulated in neural crest cells that ultimately become LTMR and proprioceptor neurons (Ma et al., 1999). In a recent study, iPSC-derived neural crest was specifically directed toward an LTMR fate with ~20% efficiency by the brief overexpression of *NGN2* and early exposure to neurotrophic factors and retinoic acid (Schrenk-Siemens et al., 2015). We took an analogous approach here, treating the cells with doxycycline for only 24 h to transiently induce NGN2-*BRN3A* expression (Figure 4A). In conjunction with the sensory neuron transcriptional program, sensory neuron subtype development and survival is influenced by exposure to retinoic acid and several neurotrophic factors: nerve growth factor (NGF), brain-derived neurotrophic factor (BDNF), glial cell line-derived neurotrophic factor (GDNF), and neurotrophin-3 (NT-3) (Airaksinen et al., 1996; Bourane et al., 2009; Carroll et al., 1998; Luo et al., 2009; Rodriguez-Tébar and Rohrer, 1991). To approximate the *in vivo* signaling milieu, we supplemented retinoic acid and all four neurotrophic factors at the same time as doxycycline, and we maintained their presence for the course of the experiment (Figure 4A). Strikingly, under these conditions, the neural crest differentiated into a homogeneous neuronal population with massive cell bodies. We will refer to these cells as neural crest-derived iSN population 2 (NC-iSN2).

Measuring the soma area of each cell population revealed the significantly larger size of NC-iSN2 relative to NC-iSN1 and the original iPSC-derived iSNs (Figure 4B). Both NC-iSN1s and NC-iSN2s were labeled by antibodies for peripherin, NEFH, and ISL1, suggesting a peripheral sensory identity (Figure 4C). Based on their large diameter, we considered that NC-iSN2s might have acquired an LTMR phenotype as reported previously (Schrenk-Siemens et al., 2015). LTMRs are specialized touch receptor neurons that lack the TRP ion channels for temperature and chemical detection. RNA *in situ* hybridization showed complete absence of *TRPM8* but a uniform expression of *PIEZO2* (Figure 4C). Consistent with an LTMR identity, NC-iSN2s exhibited rapidly adapting inward currents in response to mechanical stimulation (Figure 4D). In contrast, NC-iSN1s recapitulated the co-expression

of both *TRPM8* and *PIEZO2* originally seen in iPSC-derived iSNs (Figure 4C). Thus, simply altering the timing of developmental signals and the duration of *NGN2-BRN3A* induction can switch the neural crest fate decision between two distinct sensory neuron populations.

Transcriptomic Analysis of iSN Subtypes Derived from iPSCs and Neural Crest

Recent single-cell analyses of mouse DRG have enabled molecular classification of different sensory neuron subtypes (Chiu et al., 2014; Nguyen et al., 2017; Usoskin et al., 2015). Because our three iSN populations appear to be mostly homogeneous cultures, each of a single or a few related cell types, we applied bulk RNA sequencing to identify transcriptomic differences between iSNs, NC-iSN1s, and NC-iSN2s. We partitioned selections of genes based on existing mouse sensory neuron categories (Figure 4E; Usoskin et al., 2015). iSNs and NC-iSN1s were markedly similar, with expression of LTMR genes but lacking the LTMR-specific transcription factors *MAF* and *MAFA*. They also expressed non-overlapping sets of genes found in peptidergic nociceptors (PEPs). iSN samples were enriched for the inflammatory peptide substance P (*TAC1*) as described earlier. NC-iSN1s instead expressed the beta form of calcitonin gene-related peptide, encoded by *CALCB* (Figure 4E).

NC-iSN2s expressed LTMR genes similarly to iSNs and NC-iSN1s, but they additionally included *MAF* and *MAFA* and generally lacked expression in other subtype categories (Figure 4E). NC-iSN2s also showed selective upregulation in a group of homeobox (HOX) genes (Figure S3). HOX genes are targeted by retinoic acid signaling and encode transcription factors that control rostral-caudal neural development (Bel-Vialar et al., 2002). Supplementation of retinoic acid during motor neuron induction from embryonic stem cells shifts the positional identity from rostral to caudal via HOX gene activation, but it does not affect the overall motor neuron phenotype (Mazzoni et al., 2013). We suspect the HOX gene expression in NC-iSN2s is similarly unrelated to their LTMR phenotype, but rather is an independent effect of retinoic acid supplementation.

It is unclear whether the peripherin expression in NC-iSN2s is an artifact of *NGN2-BRN3A* programming or is a natural feature of some human LTMRs (Figures 4C and S3). In mice, anti-peripherin antibodies most strongly label medium- and small-diameter sensory neurons, with minimal labeling of large-diameter LTMRs and proprioceptors (Fornaro et al., 2008). However, *in situ* hybridization and single-cell sequencing reveal expression of peripherin mRNA in all mouse sensory neurons (Allen Mouse Spinal Cord Atlas) (Chiu et al., 2014; Nguyen et al., 2017; Usoskin et al., 2015). These data indicate that peripherin is broadly expressed in sensory ganglia and, when measured in isolation, may not reliably mark specific neuron subtypes. Also, DRG explant cultures show a drastic increase in the number of peripherin-expressing fibers, which is associated with regenerating axons (Fornaro et al., 2008). Dissociation of DRG explants further alters gene expression patterns, inducing ectopic co-expression of TrkA, TrkB, and TrkC (Genç et al., 2005). Therefore, the atypical expression of certain genes in cultured neurons, including the iSN subtypes derived here, may be an artifact of a persistent regenerative *in vitro* state. In the only other study that we

are aware of to generate human LTMR-like neurons, peripherin was not investigated (Schrenk-Siemens et al., 2015).

The retina-specific peripherin (*PRPH2*) (Arikawa et al., 1992) and motor neuron homeodomain transcription factor (*MNX1*) (Thaler et al., 1999) were absent in all three iSN culture populations, strengthening the conclusion that these iSN subtypes most closely recapitulate neurons of peripheral sensory ganglia (Figure S3). As previously noted with iPSC-derived iSNs, NC-iSN1s also expressed endogenous *NGN2* (*NEUROG2*), but NC-iSN2s did not. This persistent *NGN2* expression may be brought on by the prolonged doxycycline treatment in iSNs and NC-iSN1s. It remains to be seen whether longer-term culture after doxycycline withdrawal would extinguish the *NGN2* expression. These observations suggest that extended activation of the *NGN2-BRN3A* transgene overrides an LTMR transcriptional program, yielding an unexpected *TRPM8*$^{+}$/*PIEZO2*$^{+}$ cell type.

Some neural induction methods, including *NGN2* and *BRN3A* programming of sensory neurons directly from fibroblasts (Blanchard et al., 2015), yield a population of mixed neuronal subtypes (Wainger et al., 2015; Yang et al., 2017). To definitively establish the inter- and intra-population heterogeneity of different iSNs, we performed single-nuclei RNA sequencing on NC-iSN1s and NC-iSN2s. Individual cells from the two iSN populations were analyzed and algorithmically clustered based on transcriptional similarity (Figure 5A; see STAR Methods). NC-iSN1s and NC-iSN2s formed separate groups with little crossover, except for some NC-iSN2s that clustered among NC-iSN1s. Both conditions showed remarkable homogeneity within themselves, and no meaningful sub-clusters were identified based on differential expression of sensory genes. Inspecting single genes revealed agreement between the bulk and single-nuclei RNA sequencing. Both cell clusters expressed *SCN9A* and *PIEZO2*, only NC-iSN1s expressed *TRPM8*, and *TRPV1* was essentially absent (Figure 5B). Thus, the two neural crest-derived populations are each comprised of a distinct and homogeneous iSN subtype.

Absence of Mechanically Activated Current in iSNs from Patients with Touch and Proprioception Deficiency

One application of iPSC technology is exploring the impact of genetic variation on human physiology. We recently reported a rare sensory disorder in two unrelated individuals caused by loss-of-function mutations in *PIEZO2* (PIEZO2^{LOF}) (Chesler et al., 2016). This condition is clinically characterized in part by a profound congenital lack of proprioception, vibratory sense, and gentle touch detection on glabrous skin. To investigate sensory neuron function in this disorder, we reprogrammed iPSCs from the two PIEZO2^{LOF} patients and one unaffected sibling; the latter harbors a single apparently recessive loss-of-function allele (Table 1).

We integrated the *NGN2-BRN3A* transgene cassette, as described earlier, into the CLYBL safe-harbor locus in these iPSC lines. The iPSCs were then validated with quality-control measures alongside the healthy control line WTC11 (Figure S4). Next, we established that they could efficiently differentiate into BRN3A^{+}/ISL1^{+} iSNs (Figures S5A and S5B). All iSNs expressed TRKB and, to a lesser extent, TRKC, but not TRKA (Figures S6A and S6B). We also confirmed the presence of *PIEZO2* by *in situ* hybridization. PIEZO2^{LOF} iSNs had a noticeably diminished amount of *PIEZO2* transcript (Figure S6B). This is speculatively due

to nonsense-mediated mRNA decay, consistent with previous evaluation of PIEZO2^{LOF} patient skin biopsies (Chesler et al., 2016). Overall, iSN morphology and gene expression profile were similar across all cell lines (Figures 6A and 6B), demonstrating *NGN2-BRN3A* programming as an efficient and robust tool to derive sensory-like neurons from diverse genetic backgrounds.

To generate an isogenic control line, we used CRISPR-Cas9 to correct the putative PIEZO2^{LOF} variants in iPSCs from the second patient (Figure S7A). Corrected wild-type *PIEZO2* sequences and normal karyotype were confirmed in isolated clones (Figures S7B and S7C). Following conversion to iSNs, *in situ* hybridization on corrected cells indicated robust *PIEZO2* expression (Figure S7D). We used short tandem repeat (STR) analysis to verify that the identity of corrected iPSCs matched the unedited patient iPSCs. In the two clones tested, both showed identical STR lengths at all alleles except for the STR locus on chromosome 18, which was homozygous in the corrected clones but heterozygous in the uncorrected patient line (Table S2). In a third corrected clone, we found an abnormal karyotype due to monosomy 18 (data not shown). *PIEZO2* is located on the short arm of chromosome 18, whereas the chromosome 18 STR is located on the long arm. Based on the available evidence, we conclude that in the corrected clones with normal karyotype, one chromosome was likely corrected and subsequently duplicated, replacing the other chromosome 18. The missing copy of chromosome 18 may have become unstable because of CRISPR-Cas9-induced double-strand breaks if homology-directed repair did not occur (Lo et al., 2002). Because we were unable to isolate a biallelic corrected clone retaining each original copy of chromosome 18, we used the existing karyotypically normal clones with isodisomy 18 in the remaining experiments with this caveat in mind.

As an additional control, we generated a PIEZO2 knockout line on the genetic background of the WTC11 healthy control. Designing two CRISPR-Cas9 guide RNAs flanking *PIEZO2* exon 1 allowed for complete excision of this region on both alleles, including the start codon (Figures S7E–S7G). Producing iSNs from these knockout iPSCs, we validated the absence of *PIEZO2* mRNA transcript by *in situ* hybridization (Figure S7H).

It has been previously shown that genetic deletion of *PIEZO2* in human iPSC-derived LTMRs ablates their mechanically activated current (Schrenk-Siemens et al., 2015). If the genetic variants in PIEZO2^{LOF} patients are truly loss-of-function, we would expect the PIEZO2-dependent sensory neurons of these subjects to be similarly defective in sensing mechanical force. To test this hypothesis, we produced iSNs from all six control and patient cell lines (Table 1). We then mechanically stimulated neuron somas while recording whole-cell currents (Figure 6C). Both healthy control and unaffected sibling control iSNs reliably responded with rapid- or intermediate-adapting currents, respectively. It is unclear why recorded currents from the unaffected sibling (C2) were more challenging to stimulate to saturation and exhibited a slower adaptation rate, but the PIEZO channel family is known to display different inactivation times depending on alternative splicing or other cellular contexts (Del Mármol et al., 2018; Romero et al., 2019; Szczot et al., 2017). Variance in mechanically evoked current adaptation may also be an artifact of variability inherent to the *in vitro* differentiation system or genetic background of different cell lines. In contrast, iSNs from the two PIEZO2^{LOF} patients, as well as the *PIEZO2* knockout, were insensitive to

mechanical stimuli. Genetically corrected patient iSNs showed a complete rescue of rapidly adapting mechanically activated current (Figure 6D). Importantly, iSNs from all cell lines responded to menthol regardless of their mechanical sensitivity (Figure 6E). Our findings establish that iSNs from PIEZO2^{LOF} patients are unable to transduce mechanical force, yet they retain the gene expression profile and menthol sensitivity that are characteristic of this *in vitro* cell type.

DISCUSSION

Human sensory biology has remained largely enigmatic because of the inaccessibility of functional human nerve tissue. iPSC technology presents an opportunity to capture species- and individual-specific qualities of development, physiology, and disease *in vitro*. In this study, we used transcription factor programming to efficiently generate three separate, distinct, and homogeneous populations of peripheral sensory neurons from human iPSCs. We then applied this system to evaluate the impact of *PIEZO2* genetic variants on sensory mechanotransduction.

Existing sensory neuron differentiation techniques produce cells with heterogenous response properties (Blanchard et al., 2015; Chambers et al., 2012; Wainger et al., 2015). By overexpressing *NGN2* and *BRN3A*, a previous study by Blanchard et al. (2015) showed direct lineage conversion of mouse and human fibroblasts into iSNs at roughly 5%–10% efficiency. This method produces a mixed culture of morphologically and functionally diverse iSNs with differential responses to AITC, capsaicin, and menthol. Our approach instead harnesses the intrinsic differentiation capacity of iPSCs to produce near-pure iSN cultures. These iSNs express a specific collection of sensory genes, depending on their method of derivation, and are homogeneous in morphology and function. It will be interesting to see whether systematic application of different transcription factor combinations and developmental signals can recreate the many clinically relevant sensory neuron subtypes *in vitro*.

Several methodological variables could be responsible for the homogeneity of our iSNs and for the heterogeneity of the iSNs produced by Blanchard et al. (2015). Whereas Blanchard et al. (2015) used fibroblasts as a starting population, we used iPSCs. This difference in starting cell populations is particularly relevant because epigenetic states are known to influence the outcome of lineage reprogramming (Wapinski et al., 2013). Also, Blanchard et al. (2015) delivered the *NGN2* and *BRN3A* transcription factors on separate lentiviral vectors. We used a single genome-integrated construct expressing the two factors from the same promoter, separated by a T2A ribosomal-skipping peptide, resulting in equimolar expression of these factors. We speculate that the outcome of transcriptional programming experiments may be sensitive to the relative dosing of individual transcription factors. Methods utilizing a single factor, or factors expressed in a 1:1 ratio, often yield homogeneous cultures like the iSNs in our study (Mazzoni et al., 2013; Velasco et al., 2017; Zhang et al., 2013). Conversely, independent transmission of multiple factors, which each cell may express differently, can result in heterogenous differentiation (Benchetrit et al., 2019; Yang et al., 2017). This principle was recently demonstrated by Benchetrit et al. (2019), revealing the interplay between two transcription factors as the determinant of an

embryonic lineage decision. Future work will have to delineate the impact of transgene delivery methods on the stochasticity of cellular reprogramming.

An unexpected feature of the iSNs produced in this study is the co-expression of *TRPM8* and *PIEZO2*. It is still unclear to what degree TRPM8$^+$/PIEZO2$^+$ iSNs mimic an *in vivo* human sensory neuron subtype. Our observation that certain human DRG neurons co-express *TRPM8* and *PIEZO2* indicates that this category of cell may exist *in vivo*, despite its absence in mice (Nguyen et al., 2017; Szczot et al., 2017). Following the partial similarity of iSNs to LTMRs and their lack of nociceptor markers, we would expect *in vivo TRPM8*$^+$/*PIEZO2*$^+$ neurons to be polymodal non-nociceptive Aβ or Aδ fibers, specialized to transduce cold and mechanical stimuli. This neuron subtype could provide a molecular explanation for long-observed physiological and psychological phenomena. “Weber’s deception” is the perception that cold objects feel heavier than warmer objects (Weber, 1851). This illusion is proposed to be mediated by mechanosensory neurons that also transduce cold (Cahusac and Noyce, 2007). Classic single-fiber recordings in cat, monkey, and human sensory nerves have reported “cold-mechanoreceptors” that fit this description (Adriaensen et al., 1983; Hensel and Zotterman, 1951; Iggo and Muir, 1969; Kumazawa and Perl, 1977; Sumino and Dubner, 1981; Tapper, 1965). Given the paucity of data on human sensory ganglia (Davidson et al., 2014; Rostock et al., 2018; Zhang et al., 2015), further investigation will be critical to determine the presence of specific hitherto unrecognized cellular subtypes in humans and their similarity between commonly used animal models.

We were also surprised to observe that, in iPSC-derived neural crest, the duration of transcription factor expression influences differentiation between two sensory neuron fates. Long-term *NGN2-BRN3A* induction generates a TRPM8$^+$/PIEZO2$^+$ neuron subtype (NC-iSN1) similar to the original iSNs, whereas short-term *NGN2-BRN3A* induction leads to neurons resembling canonical LTMRs (NC-iSN2). We suggest that long-term expression of *NGN2-BRN3A* sets a transcriptional cascade of events distinct from short-term *NGN2-BRN3A* expression, ultimately activating different gene-regulatory networks. This is based on the observation that transcription factors relocate over time through synergistic interactions with other proteins (Velasco et al., 2017). This iSN model system may serve as a platform to further explore how epigenetic status and transcription factor timing shape cell fate decisions.

Here, we additionally showed that PIEZO2^{LOF} patient iSNs are completely insensitive to mechanical stimulation, but they otherwise retain all other characteristics of iSNs, including menthol responsiveness. These *in vitro* data are consistent with clinical evaluation of PIEZO2^{LOF} patients demonstrating intact thermal sensation (Chesler et al., 2016). This provides proof-of-principle that iSNs faithfully recapitulate aspects of human physiology, as reflected in the strikingly selective sensory phenotype of congenital PIEZO2 deficiency. Further, it adds direct evidence to the existing literature that PIEZO2 is the mechanotransduction channel underlying gentle touch and proprioception in humans.

The efficient derivation of homogeneous iSNs described in this study will facilitate disease studies and drug screens that rely on bulk or high-throughput approaches. Our simple induction protocol, leveraging engineered human iPSC technology, is well suited to this

purpose, obviating many culture re-plating steps and the need for complex media with small-molecule inhibitors. The iSNs reported here natively express several genes with clinical relevance for migraine and chronic pain, including *TRPM8* (Dussor and Cao, 2016), *PIEZO2* (Eijkelkamp et al., 2013; Murthy et al., 2018; Szczot et al., 2018), *TAC1* (substance P) (Sharp et al., 2006), *P2RX3* (Cook et al., 1997; Inoue et al., 2003; Sharp et al., 2006), and *SCN9A* ($Na_V1.7$) (Dib-Hajj et al., 2010). These findings set the basis for improved *in vitro* platforms where target genes can be efficiently interrogated in a sensory neuron context.

STAR ★ METHODS

LEAD CONTACT AND MATERIALS AVAILABILITY

Six human iPSC lines were generated and/or engineered for sensory neuron differentiation in this study, as detailed in Table 1. These cell lines, and the NGN2-BRN3A plasmid used for the genome engineering, are available from the Lead Contact with a Material Transfer Agreement. Information and requests for resources and reagents should be directed to and will be fulfilled by the Lead Contact, Carsten Bönnemann (carsten.bonnemann@nih.gov).

EXPERIMENTAL MODEL AND SUBJECT DETAILS

NGN2-BRN3A construct design and genomic insertion—Codon optimized human *BRN3A* was synthesized (Epoch Life Science) and subcloned into a Tet-ON 3G pUCM vector already containing a T2A-linked human *NGN2* and CLYBL homology arms, derived from the publicly available pUCM-CLYBL-hNIL plasmid (Addgene, #105841). iPSCs were transfected with Lipofectamine Stem according to manufacturer's instructions (STEM00003, Thermo Fisher) to deliver a left and right CLYBL TALEN pair (Addgene, #62196 and #62197) (Cerbini et al., 2015) with the *NGN2-BRN3A* donor construct. Clones were selected with puromycin and genotyped with three different PCR primer pairs (IDT). See Key Resources Table for a list of PCR primers used. Refer to Fernandopulle et al. (2018) for a detailed protocol on the iPSC genome engineering strategy.

iPSC reprogramming—The WTC11 control iPSC line was derived and characterized previously (Miyaoka et al., 2014). Written informed consent for patient skin biopsies was obtained by a qualified investigator (protocol 12-N-0095 approved by the National Institute of Neurological Disorders and Stroke, National Institutes of Health). Dermal fibroblasts from skin biopsies of $PIEZO2^{LOF}$ patients and an unaffected sibling (Chesler et al., 2016) were reprogrammed to iPSCs with the CytoTune-iPS 2.0 Sendai kit (Thermo Fisher, A16517) following a standard protocol described elsewhere (Beers et al., 2015). All iPSC clones were verified free of mycoplasma contamination and checked for normal karyotype after 10 passages. Karyotyping and STR analyses were performed by WiCell (Madison, WI, USA). See Key Resources Table for a list of primers (IDT) used for Sanger sequencing (GeneWiz) on $PIEZO2^{LOF}$ patient genomic DNA.

CRISPR-Cas9 editing of PIEZO2 in iPSCs—To generate the PIEZO2 knockout line, WTC11 iPSCs were dissociated in TrypLE Express, and 600,000 cells were plated per well of a 6-well plate coated with Matrigel (Corning, 354277) in 2.5 mL E8 medium with 1x RevitaCell supplement. After 30 minutes, transfection was accomplished using 4 μL

Lipofectamine Stem Reagent in 200 μL OptiMEM with 20 pmol of each modified sgRNA (Synthego) to target upstream and downstream of PIEZO2 exon 1 (5′-ACCCAGAGCCCGGTGGGCGA-3′ and 5′- TGAGTCTG GTCCGCTTTCCG-3′) and 1,800 ng eSpCas9-GFP mRNA. On the second day after transfection, GFP positive iPSCs were sorted onto Matrigel-coated 96-well plates containing 100 μL E8 Flex with 1x CloneR supplement (STEMCELL Technologies 05889) at one cell per well. Wells with surviving clones after 10 days were expanded to isolate gDNA for screening. A genomic fragment spanning the gRNA target sites was amplified using primers 5′-GCATCAGCTACCCCTGAAGA –3′ and 5′- CCAGAGCCCTTCACTTTGTT–3′ with Phusion Hot Start Flex DNA Polymerase (NEB M0535) and GC buffer and Sanger sequenced (Eurofins Genomics) to identify PIEZO2 exon 1 deletion clones. All products were from Thermo Fisher unless otherwise mentioned.

The corrected PIEZO2^{LOF} patient line was generated by the Genome Engineering and iPSC Center at Washington University School of Medicine (St. Louis, MO). Lines were created using a sgRNA cloned into an expression vector (gift from Keith Joung, Addgene plasmid 43945) co-nucleofected with Cas9 plasmid p3a-Cas9HC (gift from Jin-Soo Kim, Addgene 43945) and a single-stranded oligonucleotide donor (IDT). sgRNA sequence was 5′-GCTGACCAGAGAAATTAAGA-3′. Oligonucleotide donor sequence was (from 5′ to 3′):

ACTTGGCTTAACTCCATTTCAAGGGAGCATATTGATATATCTACAGTTCTGAGAATT
GAACGATGCATGCTGACCCGGGAAATTA
AGAAGGTAACACTGCTGGTGTAATTCTTTTTGCTCCTTCCCACATTAAGAAGACAT
TAAAAGTCA.

iPSC culture—iPSCs were maintained on tissue culture-treated polystyrene plates with Matrigel (Corning, 354277) in E8 medium (Thermo Fisher, A1517001). The medium was changed daily and the iPSCs were split every 4 – 6 days using Accutase (Invitrogen, A1110501). The rho kinase (ROCK) inhibitor 10 μM Y-27632 (Tocris, 1254) was included in the medium on the day of passaging.

Induced sensory neuron differentiation—iSNs were differentiated similarly to cortical induced neurons (Wang et al., 2017). On day 0, iPSCs were dissociated with Accutase, and 20,000 cells/cm^2 were plated on Matrigel-coated dishes in neural differentiation medium (NDM) supplemented with 10 mM Y-27632 and 2μg/mL doxycycline (Clontech, 631311). NDM (all from Invitrogen) consisted of equal parts DMEM/F12 (11330032) and Neurobasal medium (21103049), containing GlutaMAX (35050061), B27 (17504044), and N2 (17502048). The medium could be optionally changed on day 1 to remove Y-27632, but is otherwise the same composition. On day 2, the cells were dissociated with Accutase, and 50,000 cells/cm^2 were seeded on plates coated with 0.1% polyethylenimine (Sigma-Aldrich, P3143) and 15 μg/mL laminin (Invitrogen, 23017015) in NDM with doxycycline. The medium was changed every other day through day 8, after which only half volume medium changes were made. If undifferentiated cells persist, 20 μM BrdU (Sigma-Aldrich, B9285–50MG) could be optionally added on day 4 to eliminate dividing cells and achieve a pure neuronal culture. Starting on day 8 onward, neurotrophic factors (NTFs) (all R&D Systems) were added to the NDM, consisting of

BDNF (248BD025), GDNF (212GD010), β-NGF (256GF100), and NT-3 (267N3025), each at 10 ng/mL. Doxycycline was discontinued starting on day 14.

For NC-iSN1 and NC-iSN2 generation, the neural crest differentiation was a modified form of previous protocols (Bajpai et al., 2010; Schrenk-Siemens et al., 2015). On day –1 iPSCs were dissociated with Accutase and seeded in an Aggrewell 400 plate for spheroid formation (STEMCELL Technologies, 34411) according to manufacturer's instructions in E8 medium with 10 μM Y-27632. On day 0, spheroids were transferred to uncoated tissue culture-treated dishes in NDM with 20 μg/mL bFGF (R&D Systems, 233FB025), 20 μg/mL EGF (R&D Systems, 236EG200), and 10 μM of the TGF-β receptor ALK4/5/7 inhibitor SB431542 (Tocris, 1614). This medium was changed every other day. SB431542 was discontinued starting on day 6. After 1–2 weeks, spheroids spontaneously attached to the culture surface and neural crest cells migrated outward. All spheroids were manually removed, and the neural crest cells were re-plated at 40,000 cells/cm^2 on polyethylenimine and laminin-coated dishes in NDM – this is denoted as day 0 of neural induction. For NC-iSN1s, doxycycline was added from day 0 until day 14, and NTFs were supplemented beginning on day 8. For NC-iSN2s, doxycycline was added on day 0 for 24 hours. NTFs and 50 nM retinoic acid (Sigma-Aldrich, R2625) were supplemented from day 0 onward. On day 2, the neural crest cells were re-plated for the final time onto polyethylenimine and laminin-coated dishes at 50,000 cells/cm^2. Medium was changed every other day, and half medium changes were made after day 8.

METHOD DETAILS

Immunocytochemistry—Cells were washed in PBS, followed by fixation in 4% PFA for 10 minutes, and washed again in PBS prior to antibody labeling. Cells were first permeabilized with 0.25% Triton X-100 for 5 minutes and then blocked with 10% serum for up to 2 hours. Primary antibody labeling was performed overnight at 4°C in 3% serum. Primary antibody was washed and replaced with secondary antibody in 3% serum at room temperature for 60 minutes. The cells were then washed and counterstained with DAPI before mounting on slides. Images were acquired on a Nikon Eclipse Ti-E inverted microscope or on a Leica TSC SP5 II confocal microscope.

RNA *in situ* hybridization—Cells were washed with PBS, fixed for 30 minutes with 4% PFA, washed in PBS again, and serially dehydrated by increasing ethanol gradients up to 100% and stored at −20°C. *In situ* hybridization was performed with an RNAscope kit (ACD, 320851) following manufacturer's instructions. Probes were used (all ACD) against *NTRK1* (402631), *NTRK2* (402621-C2), *NTRK3* (406341-C3), *TRPM8* (543121), *TRPM8* (543121-C3), *PIEZO2* (449951), *PIEZO2* (449951-C2), and *TUBB3* (318901-C2). Images were acquired on a Leica TSC SP5 II confocal microscope with 63x objective.

For human DRG staining, we obtained tissue from three different healthy donors (Table S1) through the NIH NeuroBioBank, University of Maryland, Baltimore, MD and the Tissue for Research bank (https://biobankonline.com). Tissue from a fourth donor was purchased from AnaBios Inc., San Diego, CA (Table S1). The tissue was fresh frozen, cryosectioned, then labeled using the RNAscope kit (ACD) by manufacturer's instructions. To quench tissue

autofluorescence, sections were treated with TrueVIEW (Vector Labs) and TrueBlack (Biotium) following the manufacturer's instructions just before coverslip mounting. For quantification and the representative images in Figures S2A–S2C, DRG sections were imaged on a Nikon Eclipse Ti confocal microscope with a 40x objective. For Figure 2D, the sections were imaged on a Zeiss LSM 880 confocal microscope with a 40x objective.

RNA extraction and RT-PCR—RNA was extracted from iSNs using TRIzol (Thermo Fisher, 15596018) and chloroform and purified with an miRNeasy kit (QIAGEN, 217004) following manufacturer's instructions. Total RNA was reverse transcribed with SuperScript III (Thermo Fisher, 18080085) and ancillary reagents according to the manufacturer. The resulting cDNA was diluted to 5 ng/μL and used for end-point or quantitative PCR (qPCR). qPCR was performed in triplicate wells per sample using the Taqman Gene Expression Assay (Thermo Fisher, 4369510) on a QuantStudio 6 Flex machine (Thermo Fisher). Mock reverse-transcribed RNA was used as a negative control. End-point PCR was accomplished using an Advantage 2 PCR kit (Takara) and visualized on agarose gels. See Key Resources Table for a list of RT-qPCR and end-point PCR primers used.

Bulk RNA sequencing—Total RNA quantity and integrity were assessed on a Bioanalyzer (Agilent). For the human DRG (Clontech 636150) and iPSCs, sequencing libraries were constructed from 100 ng – 500 ng of total RNA using the TruSeq Stranded Total RNA kit (Illumina) with Ribo-Zero following the manufacturer's instructions. The fragment size of the libraries was verified using the Agilent 2100 Bioanalyzer (Agilent) and the concentrations were determined using Qubit instrument (Thermo Fisher). The libraries were loaded onto the Illumina HiSeq 3000 for 2 × 75 base pair paired-end read sequencing at approximately 40 million reads per sample. The fastq files were generated using the bcl2fastq software for further analysis. For the iSN samples, 500 ng total RNA was used in conjunction with the TruSeq Stranded Total RNA Library Prep kit (Illumina) to prepare libraries. The library quality was checked via Bioanalyzer and quantitated by Qubit (Thermo Fisher). Equimolar quantities from each library were pooled and run on a NextSeq 500/550 High Output kit v2.5 (150 cycles) (Illumina, 20024907) at approximately 40 million paired-end reads per sample.

Single-nuclei RNA sequencing—iSNs were washed in ice-cold PBS and lysed in ice-cold Nuclei EZ lysis buffer (Sigma-Aldrich, NUC-101). Samples were then filtered by a 40 μm strainer (Thermo Fisher), and centrifuged in 4°C at 800 g for 8 minutes. The pelleted nuclei were resuspended in 1% BSA in PBS, and a trypan blue-stained aliquot was counted using a hemocytometer. Nuclei were again pelleted and resuspended at a volume appropriate for the 10X Chromium system (10X Genomics). The nuclei were counted a second time to verify the quantity and to inspect the nuclei quality. 10X Chromium processing and library production were done following manufacturer's instructions. V2 chemistry and Next Gen sequencing were performed on an Illumina NextSeq 500 machine.

Calcium imaging—All calcium imaging was performed in Ringer's solution: 125 mM NaCl, 3 mM KCl, 5 mM $CaCl_2$, 1 mM $MgCl_2$, 10 mM glucose, and 10 mM HEPES (all from Sigma-Aldrich), adjusted to pH 7.3 with 1 M NaOH, and osmolality measured ~280

mmol/kg. First, cells differentiated for at least 21 days were rinsed in Ringer's solution and incubated for 1 hour at room temperature in Fluo-4 AM (Thermo Fisher, F14201) with Pluronic F-127 (Thermo Fisher, P-3000MP) in Ringer's solution following manufacturer's instructions. The cells were then rinsed in Ringer's solution and imaged in Ringer's solution at room temperature on an Olympus IX73 inverted microscope using a pco.panda sCMOS back-illuminated camera at 2 frames per second. The AMPA receptor antagonist NBQX (Tocris, 0373) was included in the imaging solution at 10 mM to prevent false positive signals from neural network activity.

All imaging trials began with 30 s of baseline measurement before the cells were exposed to chemicals or temperature-specific solutions by micropipette. The chemicals used were AITC (377430), capsaicin (M2028), menthol (M2772), α,β-meATP (M6517), and RQ-00203078 (SML1602) (all from Sigma-Aldrich). Concentrations of each chemical are noted in their respective figure legends, and temperature-specific solutions were verified by mercury thermometer prior to use.

Electrophysiology—Whole-cell currents were recorded by a Multiclamp 700B amplifier (Molecular Devices). A Digidata 1550 digitizer (Molecular Devices) was used to digitize recorded signals at 100 kHz, followed by low pass filtering at 10 kHz, and recordings were saved through Clampex 10.3 software (Molecular Devices). The bath solution was made with 133 mM NaCl, 3 mM KCl, 2.5 mM $CaCl_2$, 1 mM $MgCl_2$, 10 mM glucose, and 10 mM HEPES, adjusted to 7.3 pH with NaOH, and had an osmolality of ~280 mmol/kg. Patch pipettes were pulled and polished to a resistance of 4 – 8 MU. For current-clamp, the intracellular solution was made with 131 mM K-gluconate, 7 mM KCl, 1 mM $CaCl_2$, 1 mM $MgCl_2$, 1 mM BAPTA, 10 mM HEPES, 4 mM Mg-ATP, and 0.5 mM Na_2-GTP, adjusted to 7.3 pH with KOH, and had an osmolality of ~280 mmol/kg. Tetrodotoxin (Tocris, 1078) was bath applied at a final concentration of 500 nM. For voltage-clamp, the intracellular solution was made with 133 mM CsCl, 1 mM $CaCl_2$, 1 mM $MgCl_2$, 5 mM EGTA, 10 mM HEPES, 4 mM Mg-ATP, and 0.5 mM Na_2-GTP, adjusted to 7.3 pH with CsOH, and had an osmolality of ~275 mmol/kg. All reagents were from Sigma-Aldrich unless specifically mentioned.

Mechanical stimulation was accomplished with a blunt heat-polished pipette of 3 – 5 μm tip diameter. A P841.20 piezoelectric translator mounted on a micromanipulator (Physik Instrumente) was used to drive the pipette at a 60° angle to the culture dish. The pipette was positioned at the surface of the cell and driven in a 1 – 10 μm indentation series at 1 μm increment every 2 s, with 200 ms of indentation and a 2 ms ramp time. Only cells with less than 200 pA leak current that reached at least 6 μm of indentation before breakage of the whole-cell patch seal were kept for analysis.

Video recording of cell cultures—Time-lapse microscopy of NGN2-BRN3A engineered iPSCs (Videos S1 and S2) was performed with an IncuCyte S3 Live-Cell Analysis System. An image was acquired every 10 minutes over 72 hours then processed and exported using IncuCyte software. The mechanical stimulation assay (Video S4) was recorded on an Olympus IX73 inverted microscope using a pco.panda sCMOS back-illuminated camera with a 10 ms exposure time, and the frames were processed and exported using Fiji software.

QUANTIFICATION AND STATISTICAL ANALYSIS

Confocal microscopy analysis—Microscopy images were whole-image adjusted for brightness and contrast and quantified through Fiji software and plugins. For quantifying antibody and RNA *in situ* hybridization staining of iSNs, at least n = 3 coverslips per condition were tile-imaged, and the number of labeled cells in each fluorescent channel were counted by an observer blinded to cell line genotype. The criteria for positive RNA *in situ* hybridization staining was ≥ 5 fluorescent puncta per transcript per cell. For the analysis of human DRG dual probe RNA *in situ* hybridization experiments, whole sections of DRG were tile-imaged, and nonspecific autofluorescent background signal was removed by subtracting the fluorescence channel of probe 1 from probe 2 and vice versa. One whole section from each of n = 4 donors was quantified for *TRPM8* and *PIEZO2* probe labeling, with a cut-off of ≥ 10 fluorescent puncta per transcript constituting a positive cell.

RT-qPCR analysis—Transcript levels are expressed as cycle threshold (Ct) values as obtained from the QuantStudio 6 Flex machine software. Ct values were averaged across triplicate wells, normalized to the 60S ribosomal protein gene *RPLP0*, and multiplied by −1 for graphing purposes. Heatmaps were generated in GraphPad Prism 8.0.

Bulk RNA sequencing analysis—Fastq paired-end sequence files were first quality inspected with the FastQC tool, then adaptor clipped (TruSeq3-PE-2.fa:2:30:10) and trimmed to remove nucleotide bias (HEADCROP:11) and low quality calls (TRAILING:20 SLIDINGWINDOW:4:20 MINLEN:15) using the Trimmomatic tool (http://www.usadellab.org/cms/?page=trimmomatic). Then, the remaining intact read pairs per sample were imported into the CLCbio Genomics Workbench (https://www.qiagenbioinformatics.com) and down-sampled to 42 million reads each for the iSN samples. The iPSC and DRG samples did not require down-sampling. The reads were then reference mapped by sample to the human genome (GRCh38.82) in stranded fashion using the “RNA-Seq Analysis” tool supported under default parameters (v11). Expression for each known, annotated gene (Homo_sapiens.GRCh38.82.chr.gtf) in every sample was exported from the tool in TPM units and imported to R software for analysis (http://cran.r-project.org). In R, TPM expression was pedestalled by a value of 2 then Log_2 transformed. Transformed expression values across samples were then quantile normalized. To ensure quality of the normalized expression, and absence of sample-level outliers, exploratory inspection was performed via Tukey boxplot, covariance-based PCA scatterplot, and correlation-based heatmap. To remove noise-biased expression values, locally weighted scatterplot smoothing (LOWESS) was applied across expression for all genes separately for each sample class (Coefficient of Variation mean expression). LOWESS fits were then over-plotted and inspected to identify the common low-end expression value where the relationship between mean expression (i.e., “signal”) and Coefficient of Variation (i.e., “noise) grossly deviated from linearity (expression value = 3 for iSNs; expression value = 3.25 for iPSCs and DRG). These values were used to generate heat maps in GraphPad Prism 8.0 that were color-scaled such that genes below the noise threshold are on a blue gradient, and genes above are on a red gradient, with white representing the noise cutoff point of 3 or 3.25 TPM.

Single-nuclei RNA sequencing analysis—Sequencing data from the Illumina NextSeq 500 machine were aligned to human GRCh38.v25.premRNA-2.1.0 with CellRanger. Seurat V3.0 was used to analyze the data using standard methods described elsewhere (Butler et al., 2018).

Calcium imaging analysis—Analysis of calcium imaging videos was performed using Fiji software to draw regions of interest around randomly selected soma during the baseline period. Mean pixel intensities were measured across the entire time-lapse, and the peak intensity was extracted for each cell following each stimulus. Each value was normalized on a cell-by-cell basis by subtracting average baseline from peak intensity (ΔF) and dividing by the average baseline to achieve $\Delta F/F_0$. For individual cell scatterplots, the $\Delta F/F_0$ of each cell was further normalized to a percentage of the cell's peak KCl response.

Electrophysiology analysis—Clampfit 10.3 software (Molecular Devices) was used to visualize and quantify electrophysiological recordings. Recordings were baseline-adjusted and digitally filtered at 2 kHz before measuring peak currents from the mechanical stimulus. Individual traces and graphs were exported to GraphPad Prism 8.0 for graphing.

Statistical analysis—All statistical tests and graphs were done in GraphPad Prism 8.0 software. Data were first measured for normality by Shapiro-Wilk test. Depending on the data distribution, appropriate parametric or non-parametric one-way ANOVA methods with correction for multiple comparisons were used to determine significance. A P value of < 0.05 was used as the cut-off criteria for statistical significance when comparing two or more sets of values. The degree of statistical significance, in asterisks, is reported in each figure legend along with the number of replicates, n, used in the test. All values are expressed as means ± SEM.

Figure generation—All graphs were generated using GraphPad Prism 8.0 software. Figures were created in Adobe Illustrator 2019. The graphical abstract was created with BioRender.com.

DATA AND CODE AVAILABILITY

The bulk RNA sequencing data (GEO: GSE139273) and single-nuclei RNA sequencing data (GEO: GSE139409) from this study are publicly available at https://www.ncbi.nlm.nih.gov/geo/ using the respective accession numbers listed.

Supplementary Material

Refer to Web version on PubMed Central for supplementary material.

ACKNOWLEDGMENTS

We are grateful to the patients and their families for their participation. We would like to thank members of the Bönnemann, Chesler, and Ward labs for fruitful discussion and advice; Lars von Buchholtz for help with microscopy of human DRG; Nick Ryba and Mark Hoon for assistance with single-nuclei RNA sequencing analysis and human DRG *in situ* hybridization analysis; Zheng Wei and Daniel Martin at the NIDCR Genomics and Computational Biology Core for performing the single-nuclei RNA sequencing; and Abdel Elkahloun and Weiwei Wu at the NHGRI Sequencing Core for performing the bulk RNA sequencing. This work was supported by the

National Institutes of Health Intramural Research Program in the National Institute of Neurological Disorders and Stroke (C.G.B.) and the National Center for Complementary and Integrative Health (A.T.C.).

REFERENCES

Adriaensen H, Gybels J, Handwerker HO, and Van Hees J (1983). Response properties of thin myelinated (A-delta) fibers in human skin nerves. J. Neurophysiol 49, 111–122. [PubMed: 6298373]

Airaksinen MS, Koltzenburg M, Lewin GR, Masu Y, Helbig C, Wolf E, Brem G, Toyka KV, Thoenen H, and Meyer M (1996). Specific subtypes of cutaneous mechanoreceptors require neurotrophin-3 following peripheral target innervation. Neuron 16, 287–295. [PubMed: 8789944]

Alshawaf AJ, Viventi S, Qiu W, D'Abaco G, Nayagam B, Erlichster M, Chana G, Everall I, Ivanusic J, Skafidas E, and Dottori M (2018). Phenotypic and Functional Characterization of Peripheral Sensory Neurons derived from Human Embryonic Stem Cells. Sci. Rep 8, 603. [PubMed: 29330377]

Arikawa K, Molday LL, Molday RS, and Williams DS (1992). Localization of peripherin/rds in the disk membranes of cone and rod photoreceptors: relationship to disk membrane morphogenesis and retinal degeneration. J. Cell Biol 116, 659–667. [PubMed: 1730772]

Bai L, Lehnert BP, Liu J, Neubarth NL, Dickendesher TL, Nwe PH, Cassidy C, Woodbury CJ, and Ginty DD (2015). Genetic Identification of an Expansive Mechanoreceptor Sensitive to Skin Stroking. Cell 163, 1783–1795. [PubMed: 26687362]

Bajpai R, Chen DA, Rada-Iglesias A, Zhang J, Xiong Y, Helms J, Chang CP, Zhao Y, Swigut T, and Wysocka J (2010). CHD7 cooperates with PBAF to control multipotent neural crest formation. Nature 463, 958–962. [PubMed: 20130577]

Bandell M, Story GM, Hwang SW, Viswanath V, Eid SR, Petrus MJ, Earley TJ, and Patapoutian A (2004). Noxious cold ion channel TRPA1 is activated by pungent compounds and bradykinin. Neuron 41, 849–857. [PubMed: 15046718]

Beers J, Linask KL, Chen JA, Siniscalchi LI, Lin Y, Zheng W, Rao M, and Chen G (2015). A cost-effective and efficient reprogramming platform for large-scale production of integration-free human induced pluripotent stem cells in chemically defined culture. Sci. Rep. 5, 11319. [PubMed: 26066579]

Bel-Vialar S, Itasaki N, and Krumlauf R (2002). Initiating Hox gene expression: in the early chick neural tube differential sensitivity to FGF and RA signaling subdivides the HoxB genes in two distinct groups. Development 129, 5103–5115. [PubMed: 12399303]

Benchetrit H, Jaber M, Zayat V, Sebban S, Pushett A, Makedonski K, Zakheim Z, Radwan A, Maoz N, Lasry R, et al. (2019). Direct Induction of the Three Pre-implantation Blastocyst Cell Types from Fibroblasts. Cell Stem Cell 24, 983–994.e7. [PubMed: 31031139]

Blanchard JW, Eade KT, Szücs A, Lo Sardo V, Tsunemoto RK, Williams D, Sanna PP, and Baldwin KK (2015). Selective conversion of fibroblasts into peripheral sensory neurons. Nat. Neurosci 18, 25–35. [PubMed: 25420069]

Bourane S, Garces A, Venteo S, Pattyn A, Hubert T, Fichard A, Puech S, Boukhaddaoui H, Baudet C, Takahashi S, et al. (2009). Low-threshold mechanoreceptor subtypes selectively express MafA and are specified by Ret signaling. Neuron 64, 857–870. [PubMed: 20064392]

Butler A, Hoffman P, Smibert P, Papalexi E, and Satija R (2018). Integrating single-cell transcriptomic data across different conditions, technologies, and species. Nat. Biotechnol 36, 411–420. [PubMed: 29608179]

Cahusac PMB, and Noyce R (2007). A pharmacological study of slowly adapting mechanoreceptors responsive to cold thermal stimulation. Neuroscience 148, 489–500. [PubMed: 17683869]

Carroll P, Lewin GR, Koltzenburg M, Toyka KV, and Thoenen H (1998). A role for BDNF in mechanosensation. Nat. Neurosci 1, 42–46. [PubMed: 10195107]

Caterina MJ, Schumacher MA, Tominaga M, Rosen TA, Levine JD, and Julius D (1997). The capsaicin receptor: a heat-activated ion channel in the pain pathway. Nature 389, 816–824. [PubMed: 9349813]

Cerbini T, Funahashi R, Luo Y, Liu C, Park K, Rao M, Malik N, and Zou J (2015). Transcription activator-like effector nuclease (TALEN)-mediated CLYBL targeting enables enhanced transgene expression and one-step generation of dual reporter human induced pluripotent stem cell (iPSC) and neural stem cell (NSC) lines. PLoS ONE 10, e0116032. [PubMed: 25587899]

Chambers SM, Qi Y, Mica Y, Lee G, Zhang X-J, Niu L, Bilsland J, Cao L, Stevens E, Whiting P, et al. (2012). Combined small-molecule inhibition accelerates developmental timing and converts human pluripotent stem cells into nociceptors. Nat. Biotechnol 30, 715–720. [PubMed: 22750882]

Chesler AT, Szczot M, Bharucha-Goebel D, Čeko M, Donkervoort S, Laubacher C, Hayes LH, Alter K, Zampieri C, Stanley C, et al. (2016). The Role of PIEZO2 in Human Mechanosensation. N. Engl. J. Med 375, 1355–1364. [PubMed: 27653382]

Chiu IM, Barrett LB, Williams EK, Strochlic DE, Lee S, Weyer AD, Lou S, Bryman GS, Roberson DP, Ghasemlou N, et al. (2014). Transcriptional profiling at whole population and single cell levels reveals somatosensory neuron molecular diversity. eLife 3, e04660.

Cook SP, Vulchanova L, Hargreaves KM, Elde R, and McCleskey EW (1997). Distinct ATP receptors on pain-sensing and stretch-sensing neurons. Nature 387, 505–508. [PubMed: 9168113]

Das AT, Tenenbaum L, and Berkhout B (2016). Tet-On Systems For Doxycycline-inducible Gene Expression. Curr. Gene Ther 16, 156–167. [PubMed: 27216914]

Davidson S, Copits BA, Zhang J, Page G, Ghetti A, and Gereau RW (2014). Human sensory neurons: Membrane properties and sensitization by inflammatory mediators. Pain 155, 1861–1870. [PubMed: 24973718]

Del Mármol JI, Touhara KK, Croft G, and MacKinnon R (2018). Piezo1 forms a slowly-inactivating mechanosensory channel in mouse embryonic stem cells. eLife 7, e33149. [PubMed: 30132757]

Dhaka A, Earley TJ, Watson J, and Patapoutian A (2008). Visualizing cold spots: TRPM8-expressing sensory neurons and their projections. J. Neurosci. 28, 566–575. [PubMed: 18199758]

Dib-Hajj SD, Cummins TR, Black JA, and Waxman SG (2010). Sodium channels in normal and pathological pain. Annu. Rev. Neurosci 33, 325–347. [PubMed: 20367448]

Dussor G, and Cao YQ (2016). TRPM8 and Migraine. Headache 56, 1406–1417. [PubMed: 27634619]

Dykes IM, Tempest L, Lee S-I, and Turner EE (2011). Brn3a and Islet1 act epistatically to regulate the gene expression program of sensory differentiation. J. Neurosci 31, 9789–9799. [PubMed: 21734270]

Eijkelkamp N, Linley JE, Torres JM, Bee L, Dickenson AH, Gringhuis M, Minett MS, Hong GS, Lee E, Oh U, et al. (2013). A role for Piezo2 in EPAC1-dependent mechanical allodynia. Nat. Commun 4, 1682. [PubMed: 23575686]

Fang X, Djouhri L, McMullan S, Berry C, Okuse K, Waxman SG, and Lawson SN (2005). trkA is expressed in nociceptive neurons and influences electrophysiological properties via Nav1.8 expression in rapidly conducting nociceptors. J. Neurosci 25, 4868–4878. [PubMed: 15888662]

Fariñas I, Wilkinson GA, Backus C, Reichardt LF, and Patapoutian A (1998). Characterization of neurotrophin and Trk receptor functions in developing sensory ganglia: direct NT-3 activation of TrkB neurons in vivo. Neuron 21, 325–334. [PubMed: 9728914]

Fernandopulle MS, Prestil R, Grunseich C, Wang C, Gan L, and Ward ME (2018). Transcription Factor-Mediated Differentiation of Human iPSCs into Neurons. Curr. Protoc. Cell Biol. 79, e51. [PubMed: 29924488]

Fornaro M, Lee JM, Raimondo S, Nicolino S, Geuna S, and Giacobini-Robecchi M (2008). Neuronal intermediate filament expression in rat dorsal root ganglia sensory neurons: an in vivo and in vitro study. Neuroscience 153, 1153–1163. [PubMed: 18434031]

Genç B, Ulupinar E, and Erzurumlu RS (2005). Differential Trk expression in explant and dissociated trigeminal ganglion cell cultures. J. Neurobiol 64, 145–156. [PubMed: 15828064]

Hensel H, and Zotterman Y (1951). The response of mechanoreceptors to thermal stimulation. J. Physiol 115, 16–24. [PubMed: 14889427]

Holford LC, Case P, and Lawson SN (1994). Substance P, neurofilament, peripherin and SSEA4 immunocytochemistry of human dorsal root ganglion neurons obtained from post-mortem tissue: a quantitative morphometric analysis. J. Neurocytol 23, 577–589. [PubMed: 7529299]

Iggo A, and Muir AR (1969). The structure and function of a slowly adapting touch corpuscle in hairy skin. J. Physiol 200, 763–796. [PubMed: 4974746]

Iggo A, and Ogawa H (1977). Correlative physiological and morphological studies of rapidly adapting mechanoreceptors in cat's glabrous skin. J. Physiol 266, 275–296. [PubMed: 853451]

Inoue K, Tsuda M, and Koizumi S (2003). ATP induced three types of pain behaviors, including allodynia. Drug Dev. Res 59, 56–63.

Janssens A, Gees M, Toth BI, Ghosh D, Mulier M, Vennekens R, Vriens J, Talavera K, and Voets T (2016). Definition of two agonist types at the mammalian cold-activated channel TRPM8. eLife 5, e17240. [PubMed: 27449282]

Jones I, Yelhekar TD, Wiberg R, Kingham PJ, Johansson S, Wiberg M, and Carlsson L (2018). Development and validation of an in vitro model system to study peripheral sensory neuron development and injury. Sci. Rep 8, 15961. [PubMed: 30374154]

Jordt SE, Bautista DM, Chuang HH, McKemy DD, Zygmunt PM, Hoögestä tt ED, Meng ID, and Julius D (2004). Mustard oils and cannabinoids excite sensory nerve fibres through the TRP channel ANKTM1. Nature 427, 260–265. [PubMed: 14712238]

Knowlton WM, Palkar R, Lippoldt EK, McCoy DD, Baluch F, Chen J, and McKemy DD (2013). A sensory-labeled line for cold: TRPM8-expressing sensory neurons define the cellular basis for cold, cold pain, and cooling-mediated analgesia. J. Neurosci 33, 2837–2848. [PubMed: 23407943]

Kobayashi K, Fukuoka T, Obata K, Yamanaka H, Dai Y, Tokunaga A, and Noguchi K (2005). Distinct expression of TRPM8, TRPA1, and TRPV1 mRNAs in rat primary afferent neurons with adelta/c-fibers and colocalization with trk receptors. J. Comp. Neurol 493, 596–606. [PubMed: 16304633]

Kumazawa T, and Perl ER (1977). Primate cutaneous sensory units with unmyelinated (C) afferent fibers. J. Neurophysiol 40, 1325–1338. [PubMed: 411895]

Lallemend F, and Ernfors P (2012). Molecular interactions underlying the specification of sensory neurons. Trends Neurosci. 35, 373–381. [PubMed: 22516617]

Levanon D, Bettoun D, Harris-cerruti C, Woolf E, Negreanu V, Eilam R, Bernstein Y, Goldenberg D, Xiao C, Fliegauf M, et al. (2002). The Runx3 transcription factor regulates development and survival of TrkC dorsal root ganglia neurons. EMBO J. 21, 3454–3463. [PubMed: 12093746]

Li L, Rutlin M, Abraira VE, Cassidy C, Kus L, Gong S, Jankowski MP, Luo W, Heintz N, Koerber HR, et al. (2011). The functional organization of cutaneous low-threshold mechanosensory neurons. Cell 147, 1615–1627. [PubMed: 22196735]

Liu Z, Chen O, Wall JBJ, Zheng M, Zhou Y, Wang L, Ruth Vaseghi H, Qian L, and Liu J (2017). Systematic comparison of 2A peptides for cloning multi-genes in a polycistronic vector. Sci. Rep 7, 2193. [PubMed: 28526819]

Lo AWI, Sprung CN, Fouladi B, Pedram M, Sabatier L, Ricoul M, Reynolds GE, and Murnane JP (2002). Chromosome instability as a result of double-strand breaks near telomeres in mouse embryonic stem cells. Mol. Cell. Biol 22, 4836–4850. [PubMed: 12052890]

Luo W, Enomoto H, Rice FL, Milbrandt J, and Ginty DD (2009). Molecular identification of rapidly adapting mechanoreceptors and their developmental dependence on ret signaling. Neuron 64, 841–856. [PubMed: 20064391]

Ma Q, Fode C, Guillemot F, and Anderson DJ (1999). Neurogenin1 and neurogenin2 control two distinct waves of neurogenesis in developing dorsal root ganglia. Genes Dev. 13, 1717–1728. [PubMed: 10398684]

Marmigère F, and Ernfors P (2007). Specification and connectivity of neuronal subtypes in the sensory lineage. Nat. Rev. Neurosci. 8, 114–127. [PubMed: 17237804]

Mazzoni EO, Mahony S, Closser M, Morrison CA, Nedelec S, Williams DJ, An D, Gifford DK, and Wichterle H (2013). Synergistic binding of transcription factors to cell-specific enhancers programs motor neuron identity. Nat. Neurosci 16, 1219–1227. [PubMed: 23872598]

McKemy DD, Neuhausser WM, and Julius D (2002). Identification of a cold receptor reveals a general role for TRP channels in thermosensation. Nature 416, 52–58. [PubMed: 11882888]

Miyaoka Y, Chan AH, Judge LM, Yoo J, Huang M, Nguyen TD, Lizarraga PP, So PL, and Conklin BR (2014). Isolation of single-base genomeedited human iPS cells without antibiotic selection. Nat. Methods 11, 291–293. [PubMed: 24509632]

Moehring F, Halder P, Seal RP, and Stucky CL (2018). Uncovering the Cells and Circuits of Touch in Normal and Pathological Settings. Neuron 100, 349–360. [PubMed: 30359601]

Mu X, Silos-Santiago I, Carroll SL, and Snider WD (1993). Neurotrophin receptor genes are expressed in distinct patterns in developing dorsal root ganglia. J. Neurosci. 13, 4029–4041. [PubMed: 8366358]

Murthy SE, Loud MC, Daou I, Marshall KL, Schwaller F, Kühnemund J, Francisco AG, Keenan WT, Dubin AE, Lewin GR, et al. (2018). The mechanosensitive ion channel Piezo2 mediates sensitivity to mechanical pain in mice. Sci. Transl. Med 10, eaat9897. [PubMed: 30305457]

Nguyen MQ, Wu Y, Bonilla LS, von Buchholtz LJ, and Ryba NJP (2017). Diversity amongst trigeminal neurons revealed by high throughput single cell sequencing. PLoS ONE 12, e0185543. [PubMed: 28957441]

Peier AM, Moqrich A, Hergarden AC, Reeve AJ, Andersson DA, Story GM, Earley TJ, Dragoni I, McIntyre P, Bevan S, and Patapoutian A (2002). A TRP channel that senses cold stimuli and menthol. Cell 108, 705–715. [PubMed: 11893340]

Ranade SS, Woo SH, Dubin AE, Moshourab RA, Wetzel C, Petrus M, Mathur J, Bégay V, Coste B, Mainquist J, et al. (2014). Piezo2 is the major transducer of mechanical forces for touch sensation in mice. Nature 516, 121–125. [PubMed: 25471886]

Rodriguez-Tébar A, and Rohrer H (1991). Retinoic acid induces NGF-dependent survival response and high-affinity NGF receptors in immature chick sympathetic neurons. Development 112, 813–820. [PubMed: 1657566]

Romero LO, Massey AE, Mata-Daboin AD, Sierra-Valdez FJ, Chauhan SC, Cordero-Morales JF, and Vásquez V (2019). Dietary fatty acids finetune Piezo1 mechanical response. Nat. Commun. 10, 1200. [PubMed: 30867417]

Rostock C, Schrenk-Siemens K, Pohle J, and Siemens J (2018). Human vs. mouse nociceptors—similarities and differences. Neuroscience 387, 13–27. [PubMed: 29229553]

Schrenk-Siemens K, Wende H, Prato V, Song K, Rostock C, Loewer A, Utikal J, Lewin GR, Lechner SG, and Siemens J (2015). PIEZO2 is required for mechanotransduction in human stem cell-derived touch receptors. Nat. Neurosci 18, 10–16. [PubMed: 25469543]

Schwartzentruber J, Foskolou S, Kilpinen H, Rodrigues J, Alasoo K, Knights AJ, Patel M, Goncalves A, Ferreira R, Benn CL, et al.; HIPSCI Consortium (2018). Molecular and functional variation in iPSC-derived sensory neurons. Nat. Genet 50, 54–61. [PubMed: 29229984]

Sharp CJ, Reeve AJ, Collins SD, Martindale JC, Summerfield SG, Sargent BS, Bate ST, and Chessell IP (2006). Investigation into the role of P2X(3)/P2X(2/3) receptors in neuropathic pain following chronic constriction injury in the rat: an electrophysiological study. Br. J. Pharmacol. 148, 845–852. [PubMed: 16770326]

Sumino R, and Dubner R (1981). Response characteristics of specific thermoreceptive afferents innervating monkey facial skin and their relationship to human thermal sensitivity. Brain Res. Rev 3, 105–122.

Szczot M, Pogorzala LA, Solinski HJ, Young L, Yee P, Le Pichon CE, Chesler AT, and Hoon MA (2017). Cell-Type-Specific Splicing of Piezo2 Regulates Mechanotransduction. Cell Rep. 21, 2760–2771. [PubMed: 29212024]

Szczot M, Liljencrantz J, Ghitani N, Barik A, Lam R, Thompson JH, Bharucha-Goebel D, Saade D, Necaise A, Donkervoort S, et al. (2018). PIEZO2 mediates injury-induced tactile pain in mice and humans. Sci. Transl. Med. 10, eaat9892. [PubMed: 30305456]

Takashima Y, Daniels RL, Knowlton W, Teng J, Liman ER, and McKemy DD (2007). Diversity in the neural circuitry of cold sensing revealed by genetic axonal labeling of transient receptor potential melastatin 8 neurons. J. Neurosci 27, 14147–14157. [PubMed: 18094254]

Tapper DN (1965). Stimulus-response relationships in the cutaneous slowlyadapting mechanoreceptor in hairy skin of the cat. Exp. Neurol 13, 364–385. [PubMed: 5847283]

Thaler J, Harrison K, Sharma K, Lettieri K, Kehrl J, and Pfaff SL (1999). Active suppression of interneuron programs within developing motor neurons revealed by analysis of homeodomain factor HB9. Neuron 23, 675–687. [PubMed: 10482235]

Usoskin D, Furlan A, Islam S, Abdo H, Lönnerberg P, Lou D, HjerlingLeffler J, Haeggström J, Kharchenko O, Kharchenko PV, et al. (2015). Unbiased classification of sensory neuron types by large-scale single-cell RNA sequencing. Nat. Neurosci 18, 145–153. [PubMed: 25420068]

Vang H, Chung G, Kim HY, Park S-B, Jung SJ, Kim J-S, and Oh SB (2012). Neurochemical properties of dental primary afferent neurons. Exp. Neurobiol 21, 68–74. [PubMed: 22792027]

Velasco S, Ibrahim MM, Kakumanu A, Garipler G, Aydin B, Al-Sayegh MA, Hirsekorn A, Abdul-Rahman F, Satija R, Ohler U, et al. (2017). A Multi-step Transcriptional and Chromatin State Cascade Underlies Motor Neuron Programming from Embryonic Stem Cells. Cell Stem Cell 20, 205–217.e8. [PubMed: 27939218]

Wainger BJ, Buttermore ED, Oliveira JT, Mellin C, Lee S, Saber WA, Wang AJ, Ichida JK, Chiu IM, Barrett L, et al. (2015). Modeling pain in vitro using nociceptor neurons reprogrammed from fibroblasts. Nat. Neurosci 18, 17–24. [PubMed: 25420066]

Wang C, Ward ME, Chen R, Liu K, Tracy TE, Chen X, Xie M, Sohn PD, Ludwig C, Meyer-Franke A, et al. (2017). Scalable Production of iPSC-Derived Human Neurons to Identify Tau-Lowering Compounds by High-Content Screening. Stem Cell Reports 9, 1221–1233. [PubMed: 28966121]

Wapinski OL, Vierbuchen T, Qu K, Lee QY, Chanda S, Fuentes DR, Giresi PG, Ng YH, Marro S, Neff NF, et al. (2013). Hierarchical mechanisms for direct reprogramming of fibroblasts to neurons. Cell 155, 621–635. [PubMed: 24243019]

Weber EH (1851). Tastsinn und Gemeingefühl (Leipzig: Wilhelm Engelmann).

Wende H, Lechner SG, Cheret C, Bourane S, Kolanczyk ME, Pattyn A, Reuter K, Munier FL, Carroll P, Lewin GR, and Birchmeier C (2012). The Transcription Factor c-Maf Controls Touch Receptor Development and Function. Science 335, 1373–1376. [PubMed: 22345400]

Woo S-H, Lukacs V, de Nooij JC, Zaytseva D, Criddle CR, Francisco A, Jessell TM, Wilkinson KA, and Patapoutian A (2015). Piezo2 is the principal mechanotransduction channel for proprioception. Nat. Neurosci 18, 1756–1762. [PubMed: 26551544]

Yang N, Chanda S, Marro S, Ng YH, Janas JA, Haag D, Ang CE, Tang Y, Flores Q, Mall M, et al. (2017). Generation of pure GABAergic neurons by transcription factor programming. Nat. Methods 14, 621–628. [PubMed: 28504679]

Zhang Y, Pak C, Han Y, Ahlenius H, Zhang Z, Chanda S, Marro S, Patzke C, Acuna C, Covy J, et al. (2013). Rapid single-step induction of functional neurons from human pluripotent stem cells. Neuron 78, 785–798. [PubMed: 23764284]

Zhang XL, Lee KY, Priest BT, Belfer I, and Gold MS (2015). Inflammatory mediator-induced modulation of GABAA currents in human sensory neurons. Neuroscience 310, 401–409. [PubMed: 26415765]

Highlights

- *NGN2-BRN3A* expression in human stem cells induces homogeneous sensory neurons (iSNs)
- Three kinds of iSNs can be produced, including subtypes coexpressing *TRPM8* and *PIEZO2*
- *TRPM8* and *PIEZO2* unexpectedly mark a subset of sensory neurons in humans, but not mice
- iSNs from PIEZO2-deficient patients are insensitive to mechanical stimuli

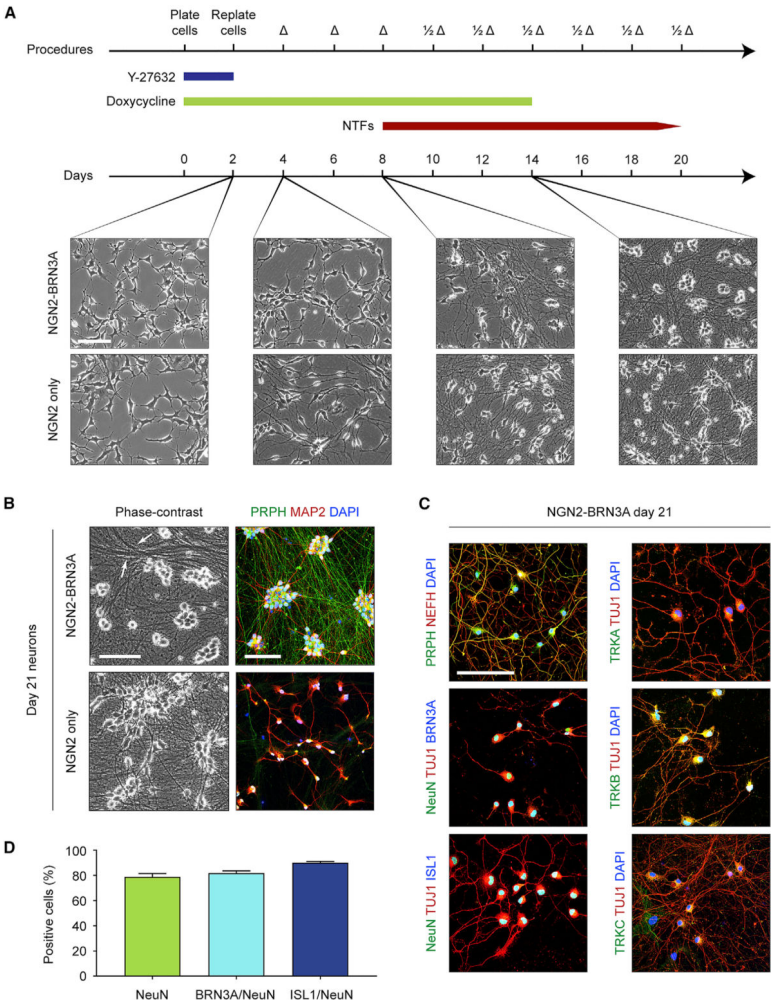

Figure 1. ***NGN2-BRN3A*** **Programming of Human iPSCs Efficiently Yields Induced Sensory Neurons**

(A) Protocol for sensory neuron induction using *NGN2-BRN3A*-engineered iPSCs. Phase-contrast images were captured on days 2, 4, 8, and 14 after doxycycline addition. Neurons induced with *NGN2* alone are shown on the bottom for comparison.

(B) Phase-contrast and immunocytochemistry images of day 21 neurons induced by *NGN2-BRN3A* and *NGN2* only.

(C) Immunocytochemistry of day 21 *NGN2-BRN3A* neurons to detect proteins found in sensory neurons.

(D) Quantification of percent staining NeuN (78.9% ± 2.6%), BRN3A/NeuN (82.0% ± 1.7%), and ISL1/NeuN (90.1% ± 1.0%). For NeuN stains, n = 6 independent coverslips were used and were split for co-staining into n = 3 coverslips for BRN3A and n = 3 for ISL1. At least 200 cells were counted per stain. Values are expressed as mean ± SEM. Scale bars, 100 μm.

Δ, medium change; 1/2Δ, half medium change; NTF, neurotrophic factor; Y-27632, ROCK inhibitor. See also Figure S1 and Videos S1 and S2.

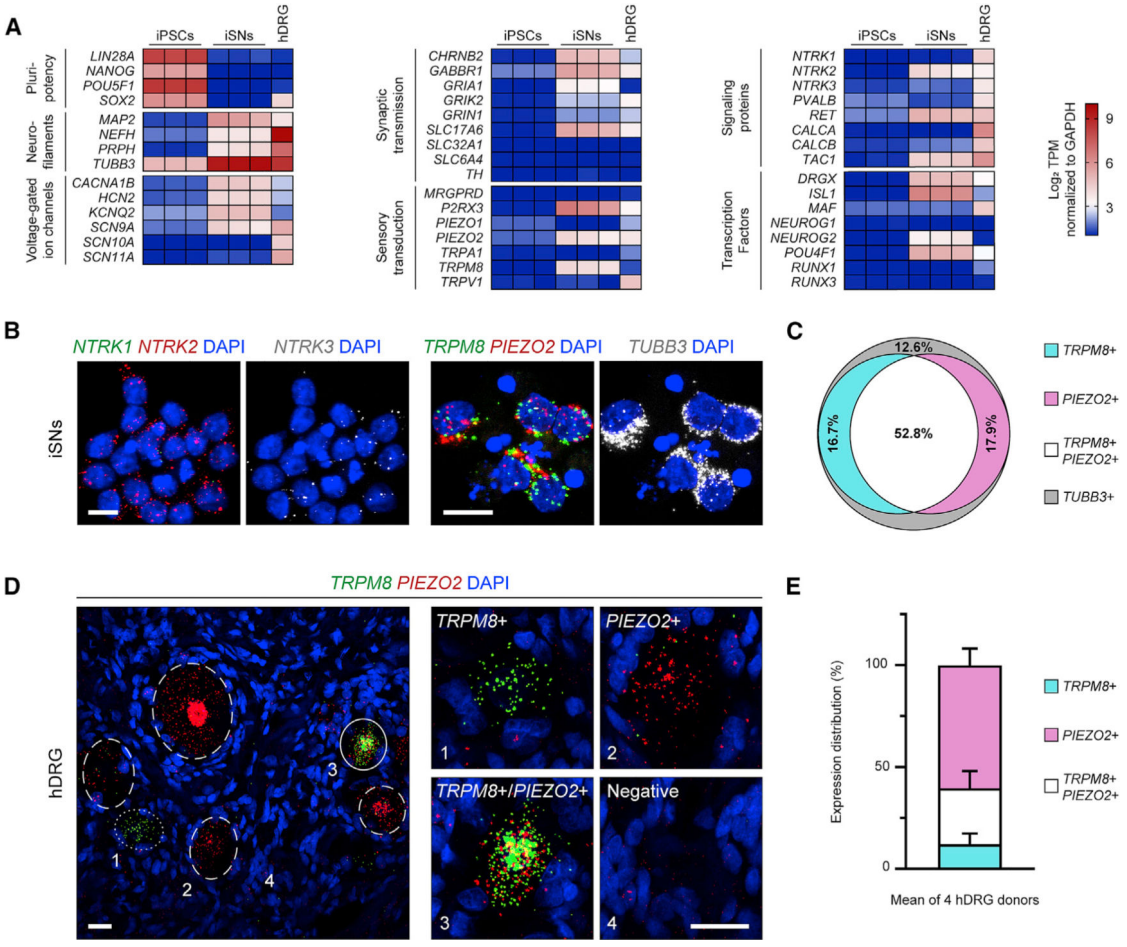

Figure 2. iSNs and Human DRG Neurons Co-express *TRPM8* and *PIEZO2*

(A) Heatmap of RNA sequencing results on iPSCs, iSNs, and adult human donor DRG (hDRG). Each column represents an individual sample's normalized $\log_2$ transcripts per million (TPM). The hDRG is a pooled RNA sample from 21 individuals.

(B) RNA *in situ* hybridization on iSNs for transcripts of neurotrophin and sensory receptors. Each small fluorescent punctum roughly indicates one transcript. *TUBB3* encodes a general neuron class of microtubule, βIII-tubulin. Scale bars, 10 μm.

(C) Quantification of *in situ* hybridization in iSNs using a cutoff criteria of ≥ 5 puncta per transcript for positive cells. *TRPM8*$^+$ (17.9% ± 1.5%), *PIEZO2*$^+$ (14.0% ± 4.6%), *TRPM8*$^+$/*PIEZO2*$^+$ (56.0% ± 6.3%), and *TUBB3*$^+$ only (11.5% ± 3.4%). 199 cells were counted across n = 5 coverslips.

(D) RNA *in situ* hybridization for *TRPM8* and *PIEZO2* in human DRG (hDRG). Labeled neurons are shown in wide-field view (left) with dotted, dashed, and solid circles indicating *TRPM8*$^+$, *PIEZO2*$^+$, and *TRPM8*$^+$/*PIEZO2*$^+$ neurons, respectively. Zoomed images of single neurons (right), individually marked by numbers in the wide-field view. Scale bars, 25 μm.

(E) Quantification of human DRG *in situ* hybridization. *TRPM8*$^+$ (12.8% ± 4.4%), *PIEZO2*$^+$ (59.7% ± 6.8%), and *TRPM8*$^+$/*PIEZO2*$^+$ (27.4% ± 6.9%). 622 positive cells were counted across n = 4 DRG donors. All values are expressed as mean ± SEM.

See also Figure S2 and Table S1.

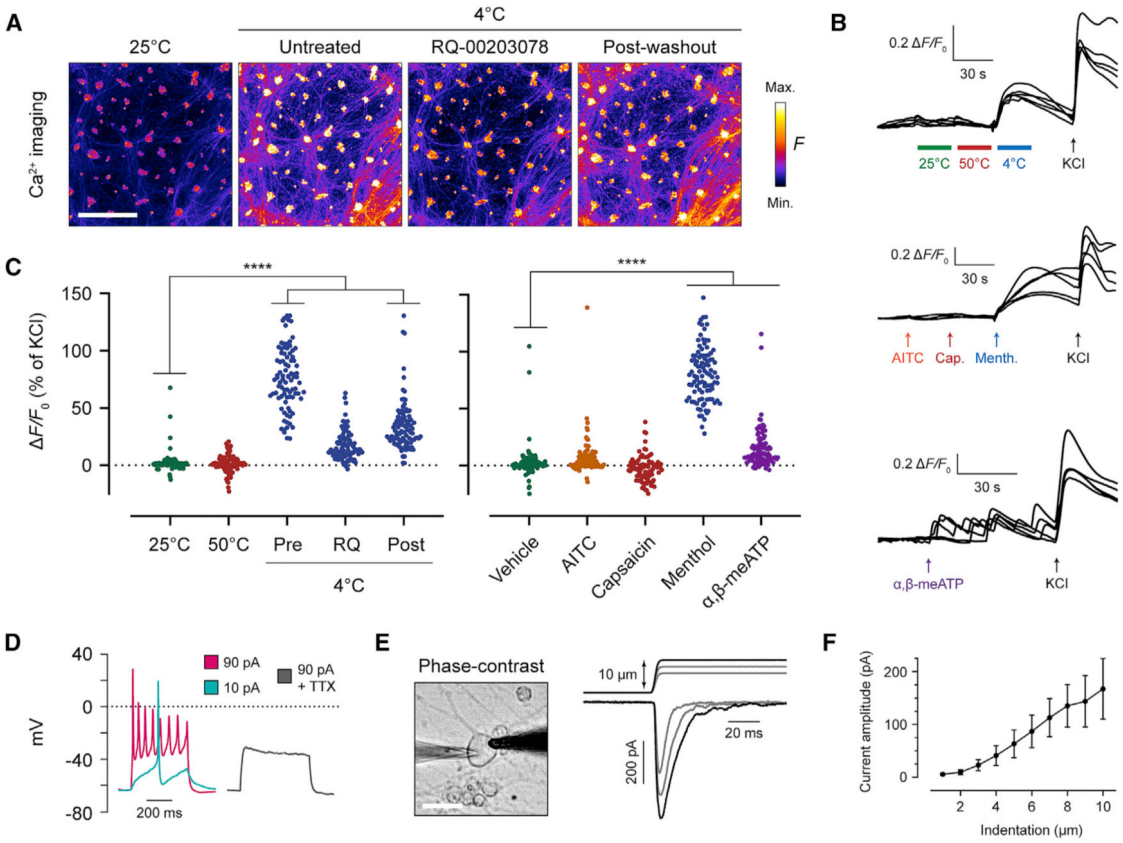

Figure 3. iSNs Detect Cold Temperature and Mechanical Force

(A) Fluo-4 fluorescence images recording iSNs at 25°C and 4°C. The TRPM8 inhibitor RQ-00203078 was incubated at 10 μM for 5 min before resuming recording. A 5-min room temperature incubation was used in between each 4°C treatment. Scale bar, 500 μm.

(B) Representative fluorescence traces of calcium imaging trials, with 5 cells shown per trial. Values are graphed as the change in fluorescence intensity from baseline and divided by the baseline ($\Delta F/F_0$). 100 μM AITC, 10 μM capsaicin, 500 μM menthol, and 50 μM α,β-methylene-ATP (α,β-meATP) were used.

(C) Scatter dot plots of peak $\Delta F/F_0$ of individual cells after application of temperature or chemicals. Each cell is normalized to a percentage of its own KCl response at the end of the recording period. For each condition, ≥ 80 cells were analyzed. Post hoc comparisons of each treatment to vehicle with one-way ANOVA and Dunnett's correction for multiple comparisons. p values: 50°C, p = 0.99; 4°C pre, p = 0.0001; 4°C RQ, p = 0.5135; 4°C post, p = 0.001; AITC, p = 0.1379; capsaicin, p = 0.5242; menthol, p = 0.0001; α,β-meATP, p = 0.0001. ****p < 0.0001.

(D) Example whole-cell current-clamp recording of iSNs in response to depolarizing currents. A total of n = 4 cells were recorded without tetrodotoxin (TTX) andn = 5 cells with 1 μM TTX.

(E) Mechanical stimulation of iSNs in whole-cell voltage-clamp mode. In the phase-contrast image, the recording pipette is on the left, and the stimulator probe is on the right. Scale bar, 20 μm. In the recording, the top trace indicates micrometer steps of the stimulator probe, whereas the bottom trace shows whole-cell currents.

(F) Quantification of the current amplitude at each probe indentation depth. A total of n = 10 cells were recorded, with 10/10 cells displaying a peak mechanically evoked current above 50 pA. Values are expressed as mean ± SEM.

See also Videos S3 and S4.

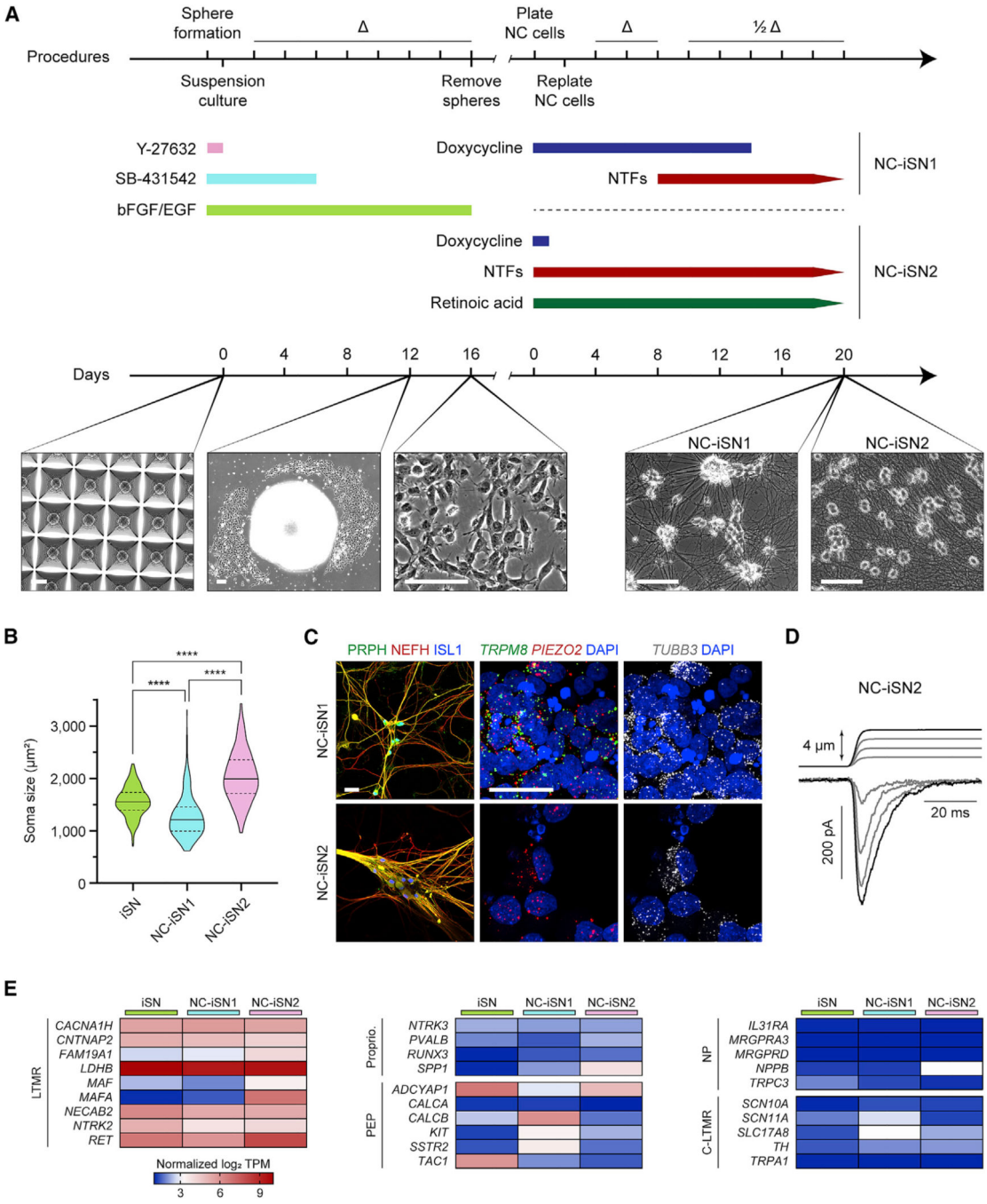

Figure 4. Varied Induction of *NGN2-BRN3A* in Neural Crest Yields Divergent Sensory Neuron Populations

(A) Protocol and phase-contrast images of neural crest differentiation with two strategies for sensory neuron induction (NC-iSN1 and NC-iSN2). Day 0 depicts neurectodermal spheroid formation in a microwell plate. Day 12 shows neural crest migration from an individual spheroid. Scale bars, 100 µm.

(B) Quantification of cell soma area based on phase-contrast images across three differentiation experiments of iSNs (n = 301 cells), NC-iSN1s (n = 228 cells), and NC-

iSN2s (n = 332 cells). Values are expressed as mean ± SEM. Post hoc comparisons with Kruskal-Wallis test and Dunn's correction for multiple comparisons, ****$p < 0.0001$.

(C) Representative immunohistochemistry and RNA *in situ* hybridization experiments on NC-iSN1s and NC-iSN2s. Scale bars, 25 μm.

(D) Representative mechanical stimulation of NC-iSN2s in whole-cell voltage-clamp. A total of n = 6 cells were recorded.

(E) RNA sequencing heatmap expression results of selected genes grouped by known sensory neuron subtype. Each heatmap column depicts the average $\log_2$ TPM of three independent samples.

Δ, medium change; 1/2Δ, half medium change; C-LTMR, C fiber LTMR; LTMR, low-threshold mechanoreceptor; NC, neural crest; NP, nonpeptidergic nociceptor; PEP, peptidergic nociceptor; Proprio., proprioceptor. See also Figure S3.

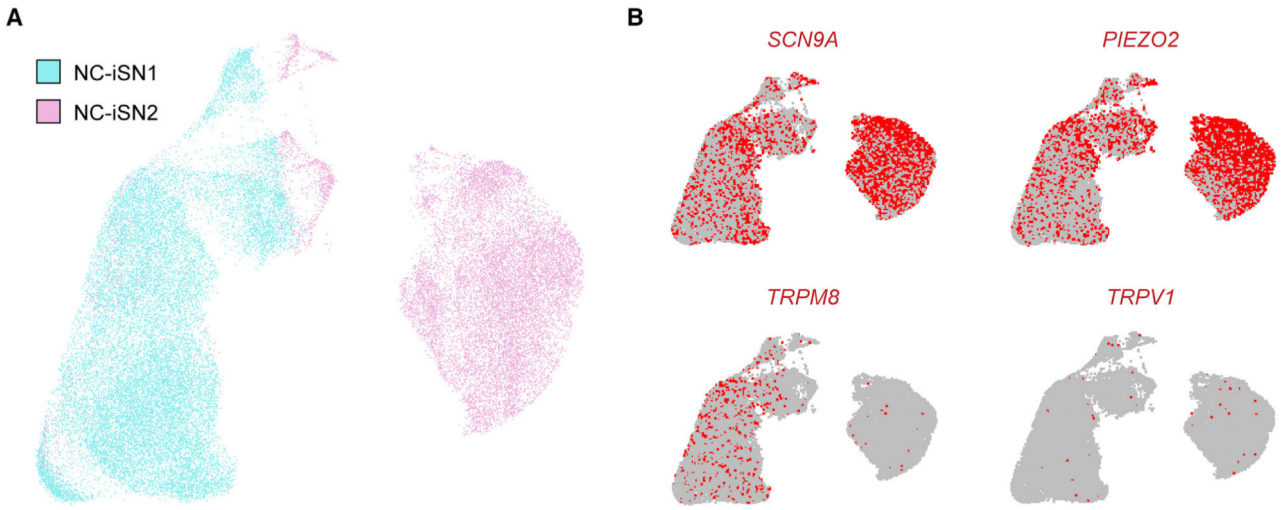

Figure 5. Single-Cell RNA Sequencing of Neural Crest-Derived iSNs

(A) Merged UMAP plot representing individual cells from a single differentiation of both NC-iSN1 (22,804 cells) and NC-iSN2 (15,004 cells).

(B) Expression UMAP plots indicating cells in the upper 90% of the population distribution with mapped reads to specific genes, based on unique molecular identifier counts.

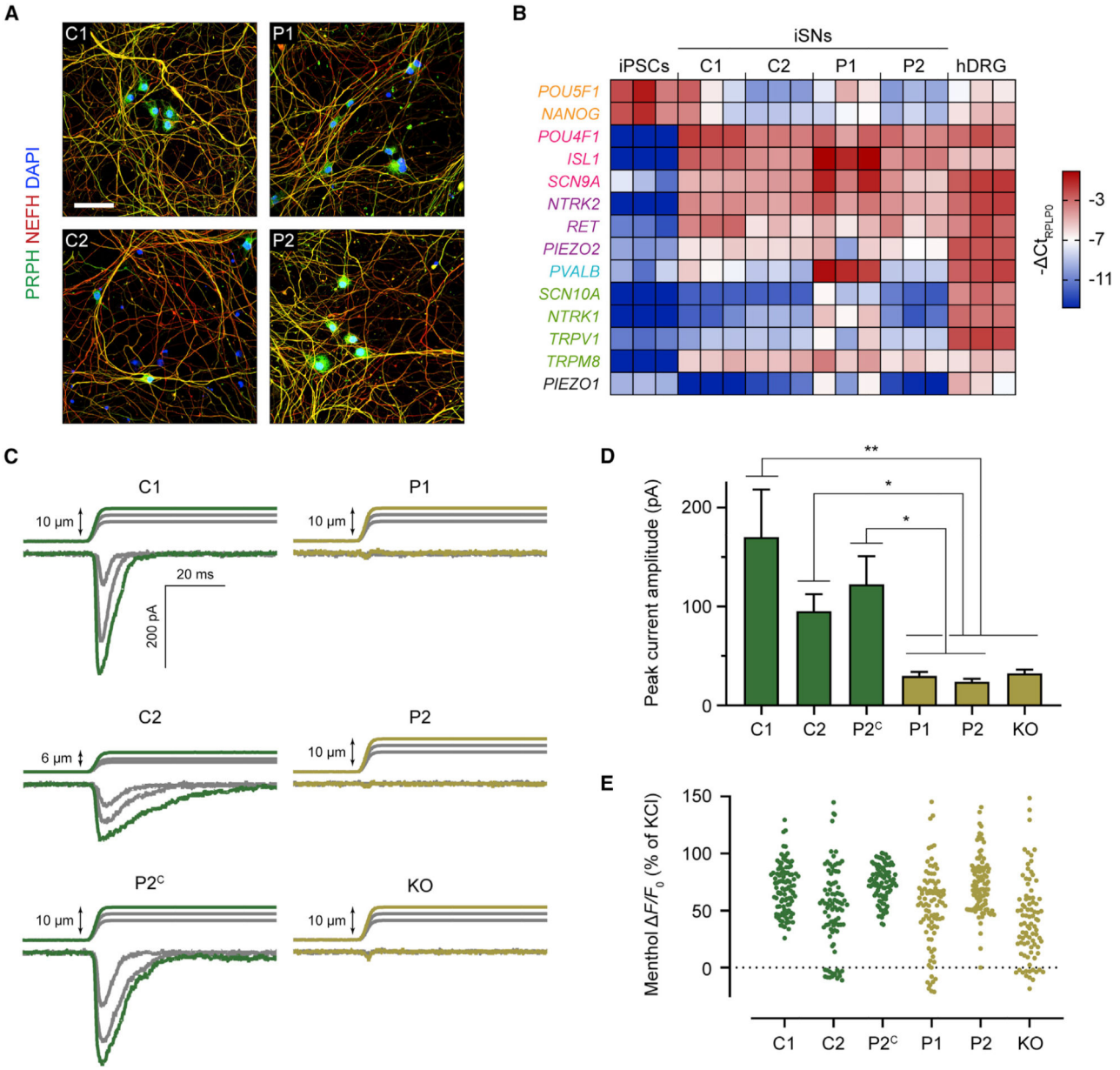

Figure 6. PIEZO2^{LOF} iSNs Are Insensitive to Mechanical Stimuli

(A) Representative immunocytochemistry from at least three differentiations of control and patient iSNs. Scale bar, 50 µm.

(B) qRT-PCR of sensory-related genes in day 21 iSNs, normalized to the housekeeping gene *RPLP0* and expressed as −ΔCt for color coding. Each column represents an independent sample, three samples per cell line. Human DRG (hDRG) total RNA was used as a positive control, and WTC11 iPSCs were used as a negative control. Text color denotes gene category: orange, pluripotency; magenta, pan-sensory; purple, LTMR; blue, proprioceptor; green, nociceptor and/or thermoreceptor.

(C) Whole-cell voltage-clamp recordings of iSNs during mechanical stimulation. Traces are examples from n = 10 neurons for each cell line.

(D) Quantification of mechanically activated current peak amplitudes in n = 10 cells per cell line. Values are expressed as mean ± SEM. Post hoc comparisons with Kruskal-Wallis test and Dunn's correction for multiple comparisons. *p < 0.05, **p < 0.01.
(E) Scatter dot plot for peak $\Delta F/F_0$ of individual cells after exposure to 500 μM menthol, normalized to KCl response. For each cell line, ≥80 cells were analyzed. In post hoc comparisons between each sample with one-way ANOVA and Dunnett's correction for multiple comparisons, no comparison was significantly different (p > 0.05).
See also Figures S4–S7 and Table S2.

Table 1.

Summary of Human iPSC Lines

Name	Donor Identity	Genotype	Donor Age	Donor Gender	Donor Ancestry
C1	healthy control 1	wild type	30 years	male	Japanese
C2	healthy sibling of P1	heterozygous recessive *PIEZO2* mutation c.4723C>T	21 years	female	Bangladeshi
P1	PIEZO2 patient 1	compound heterozygous *PIEZO2* mutations c.4723C>T and c.5053C>T	19 years	female	Japanese/European
P2	PIEZO2 patient 2	compound heterozygous *PIEZO2* mutations c.5054G>C and c.5053C>T	10 years	female	Bangladeshi
$P2^{C}$	PIEZO2 patient 2	CRISPR-Cas9-mediated *PIEZO2* correction in patient 2 iPSCs	see P2		
KO	healthy control 1	CRISPR-Cas9-mediated *PIEZO2* knockout in control 1 iPSCs	see C1		

KEY RESOURCES TABLE

REAGENT or RESOURCE	SOURCE	IDENTIFIER
Antibodies		
Peripherin	Abcam	ab4666; RRID: AB_449340
MAP2	Abcam	ab5392; RRID: AB_2138153
NEFH	Abcam	ab72996; RRID: AB_2149618
TUJ1 (mouse)	Abcam	ab78078; RRID: AB_2256751
TUJ1 (chicken)	Abcam	ab107216; RRID: AB_10899689
NeuN	Abcam	ab104225; RRID: AB_10711153
BRN3A	Millipore	MAB1585; RRID: AB_94166
ISL1	DSHB	40.2D6; RRID: AB_528315
TRKA	Abcam	ab76291; RRID: AB_1524514
TRKB	Alomone Labs	ANT-019-AG; RRID: AB_10917156
TRKC	OriGene	TA336908
OCT4	Abcam	ab19857; RRID: AB_445175
SSEA4	STEMCELL Technologies	60062
NANOG	ReproCELL	RCAB0004P-F; RRID: AB_567470
TRA-1–81	Millipore	MAB4381; RRID: AB_177638
SOX2	Thermo Fisher	PA1–16968; RRID: AB_2195781
TRA-1–60	Millipore	MAB4360; RRID: AB_2119183
Chemicals, Peptides, and Recombinant Proteins		
Y-27632	Tocris	1254
Doxycycline	Clontech	631311
BDNF	R&D Systems	248BD025
GDNF	R&D Systems	212GD010
β-NGF	R&D Systems	256GF100
NT-3	R&D Systems	267N3025
bFGF	R&D Systems	233FB025
EGF	R&D Systems	236EG200
SB431542	Tocris	1614
Retinoic acid	Sigma-Aldrich	R2625
AITC	Sigma-Aldrich	377430
Capsaicin	Sigma-Aldrich	M2028
Menthol	Sigma-Aldrich	M2772
α,β-meATP	Sigma-Aldrich	M6517
RQ-00203078	Sigma-Aldrich	SML1602
Tetrodotoxin	Tocris	1078
Critical Commercial Assays		

REAGENT or RESOURCE	SOURCE	IDENTIFIER
Taqman Gene Expression Assay	Thermo Fisher	18080085
Taqman RT-qPCR probes (see Oligonucleotides below)	Thermo Fisher	N/A
RNAscope® Fluorescent Multiplex Detection Reagents	ACD	320851
RNAscope® Probe – Hs-TRPM8	ACD	543121
RNAscope® Probe – Hs-TRPM8-C3	ACD	543121-C3
RNAscope® Probe – Hs-PIEZO2	ACD	449951
RNAscope® Probe – Hs-PIEZO2-C2	ACD	449951-C2
RNAscope® Probe – Hs-NTRK1	ACD	402631
RNAscope® Probe – Hs-NTRK2-C2	ACD	402621-C2
RNAscope® Probe – Hs-NTRK3-C3	ACD	406341-C3
RNAscope® Probe – Hs-TUBB3-C2	ACD	318901-C2
Deposited Data		
Bulk RNA sequencing data	https://www.ncbi.nlm.nih.gov/geo/	Accession GSE139273
Single-nuclei RNA sequencing data	https://www.ncbi.nlm.nih.gov/geo/	Accession GSE139409
Experimental Models: Cell Lines		
WTC11 iPSC	Miyaoka et al., 2014	Coriell GM25256
WTC11 NGN2 iPSC	Wang et al., 2017	N/A
WTC11 NGN2-BRN3A iPSC (C1)	This study	N/A
WTC11 NGN2-BRN3A iPSC, PIEZO2 knockout (KO)	This study	N/A
PIEZO2 patient 1 NGN2-BRN3A iPSC (P1)	This study	N/A
PIEZO2 patient 1 healthy sibling NGN2-BRN3A iPSC (C2)	This study	N/A
PIEZO2 patient 2 NGN2-BRN3A iPSC (P2)	This study	N/A
PIEZO2 patient 2 NGN2-BRN3A iPSC, CRISPR-Cas9-corrected ($P2^{C}$)	This study	N/A
Oligonucleotides		
CLYBL wild type genotyping primer, forward: 5′-TGACTAAACACTGT GCCCCA-3′	This study	N/A
CLYBL wild type genotyping primer, reverse: 5′-AGGCAGGATGAAT TGGTGGA-3′	This study	N/A
CLYBL 5′ insert genotyping primer, forward: 5′-CAGACAAGTCAGT AGGGCCA-3′	This study	N/A
CLYBL 5′ insert genotyping primer, reverse: 5′-AGAAGACTTCCTCT GCCCTC-3′	This study	N/A
CLYBL 3′ insert genotyping primer, forward: 5′-GGTAGGAAGTGGT ACGGAAA-3′	This study	N/A
CLYBL 3′ insert genotyping primer, reverse: 5′-GAACGATTTACTGG GCAGTC-3′	This study	N/A
NGN2-BRN3A transgene RT-PCR primer, forward: 5′-CAAGATC GAAACCCTGAGAT-3′	This study	N/A
NGN2-BRN3A transgene RT-PCR primer, reverse: 5′-GATGGGTAC TTATGCTCAGG-3′	This study	N/A
PIEZO2 exon 32 sequencing primer, forward: 5′-AGACCCAATAT GCCAACACC-3′	Chesler et al., 2016	N/A

REAGENT or RESOURCE	SOURCE	IDENTIFIER
PIEZO2 exon 32 sequencing primer, reverse: 5′-GGGAGCAGGCA TCATTACAA-3′	Chesler et al., 2016	N/A
PIEZO2 exon 35 sequencing primer, forward: 5′-GGTAAAACATC GCTGGGCTA-3′	Chesler et al., 2016	N/A
PIEZO2 exon 35 sequencing primer, reverse: 5′-AAGGGGTTATG CCACAACTG-3′	Chesler et al., 2016	N/A
RT-qPCR primer - RPLP0	IDT	Hs.PT.39a.22214824
RT-qPCR primer - ISL1	Thermo Fisher	Hs00158126_m1
RT-qPCR primer - POU4F1	Thermo Fisher	Hs00366711_m1
RT-qPCR primer - NTRK1	Thermo Fisher	Hs01021011_m1
RT-qPCR primer - NTRK2	Thermo Fisher	Hs00178811_m1
RT-qPCR primer - PIEZO1	Thermo Fisher	Hs00207230_m1
RT-qPCR primer - PIEZO2	Thermo Fisher	Hs00926218_m1
RT-qPCR primer - SCN9A	Thermo Fisher	Hs00161567_m1
RT-qPCR primer - SCN10A	Thermo Fisher	Hs01045137_m1
RT-qPCR primer - RET	Thermo Fisher	Hs01120030_m1
RT-qPCR primer - MAF	Thermo Fisher	Hs04185012_s1
RT-qPCR primer - PVALB	Thermo Fisher	Hs00161045_m1
RT-qPCR primer - TRPV1	Thermo Fisher	Hs00218912_m1
RT-qPCR primer - TRPM8	Thermo Fisher	Hs01066596_m1
RT-qPCR primer - SOX10	Thermo Fisher	Hs00366918_m1
RT-qPCR primer - PAX3	Thermo Fisher	Hs00240950_m1
RT-qPCR primer - POU5F1	Thermo Fisher	Hs00999632_g1
RT-qPCR primer - NANOG	Thermo Fisher	Hs02387400_g1
Recombinant DNA		
pUCM-CLYBL-NGN2-BRN3A	This study	N/A
pZT-C13-L1	Cerbini et al., 2015	Addgene #62196
pZT-C13-R1	Cerbini et al., 2015	Addgene #62197